

Fatigue detection via sequential testing of biomechanical data using martingale statistic

Rupsa Basu¹ and Katharina Proksch¹

¹Faculty of Electrical Engineering, Mathematics and Computer Science,
Universiteit Twente, Enschede, The Netherlands.

June 5, 2023

Abstract

Injuries to the knee joint are very common for long-distance and frequent runners, an issue which is often attributed to fatigue. We address the problem of fatigue detection from biomechanical data from different sources, consisting of lower extremity joint angles and ground reaction forces from running athletes with the goal of better understanding the impact of fatigue on the biomechanics of runners in general and on an individual level. This is done by sequentially testing for change in a datastream using a simple martingale test statistic. Time-uniform probabilistic martingale bounds are provided which are used as thresholds for the test statistic. Sharp bounds can be developed by a hybrid of a piece-wise linear- and a law of iterated logarithm- bound over all time regimes, where the probability of an early detection is controlled in a uniform way. If the underlying distribution of the data gradually changes over the course of a run, then a timely upcrossing of the martingale over these bounds is expected. The methods are developed for a setting when change sets in gradually in an incoming stream of data. Parameter selection for the bounds are based on simulations and methodological comparison is done with respect to existing advances. The algorithms presented here can be easily adapted to an online change-detection setting. Finally, we provide a detailed data analysis based on extensive measurements of several athletes and benchmark the fatigue detection results with the runners' individual feedback over the course of the data collection. Qualitative conclusions on the biomechanical profiles of the athletes can be made based on the shape of the martingale trajectories even in the absence of an upcrossing of the threshold.

Keywords: Time series, sequential & online testing, biomechanical data analysis, fatigue detection, change point detection, martingales, sports data

1 Introduction

The past decades have seen an immense increase in data collection, processing, analysis and storage concerning almost all aspects of science and technology. Many modern data

sets are too large or complex to be analyzed by traditional approaches, in particular if the goal is to use as much of the information provided by the data as quickly as possible. Additionally, some applications require for the information to be processed real-time in which case new methods have to be devised with the capability to relay results ‘on the fly’. And while the amount of data is ever increasing, attempts have to be constantly made to not only update pre-existing methods for analysing them but also to ensure that the computational time and memory usage needed are lesser than before. For example, with the advent of wearable devices in sports and other biomechanical applications, the RAM capabilities of such devices are often limited. Further, present day scientific research is multidisciplinary with subject areas under consideration being studied by members and teams of wide-ranging fields. Therefore, for applications of theoretical methods of one area, techniques applied should be well comprehensible by experts from other fields. In this paper, we focus on some crucial questions regarding statistical analysis of biomechanics of human movement, with applications particularly in data obtained from running athletes.

The research question pursued in this work pertains to addressing fatigue detection in biomechanical sports data obtained from running athletes. In particular, fatigue changes the movement pattern of a runner, hereby increasing the risk of overloading or getting injured. Hence, the goal is to identify the changes undergone in the body when subjected to fatigue as a consequence of prolonged running. There has been an increasing trend to monitor biomechanical movement patterns due to wide application areas including but not restricted to; engineering (Postema et al. (1997)), clinical (Lu and Chang (2012)), rehabilitation (Yoshioka et al. (2009)) and sports applications (Zandbergen et al. (2022)). Understanding general movement during sports performance may be done by making use of several devices, in particular activity trackers like smart watches, measuring parameters such as the heart rate of an athlete, or even more complex body worn (inertial) sensors, or in special laboratory setting with force-plates integrated into treadmills and bio-marker sets on the walls (all of which are included in this work). Running has been an immensely popular recreational sport worldwide over the past decades, with a large number of people suffering from running related injuries; see, Scheerder et al. (2015), Buist et al. (2010) and Zandbergen et al. (2023) for further references. To address this problem, appropriate study of the biomechanical data obtained from lower extremity joints (most susceptible to injuries) is required.

This paper presents a case study based on a data set collected within the multidisciplinary project *Sports, Data, and Interaction*¹. Data collection was designed in such a manner that it is ensured that the athlete taking part in the study would surely but steadily get tired during the course of the run. Such a protocol to obtain fatigue data can be designed in a variety of ways, for example as in Apte et al. (2021). In our setting, the runners were asked for their average speed in an 8 km run and the speed of the experi-

¹<http://www.sports-data-interaction.com/>

mental design for data collection would be adjusted to 103% of this value, ensuring fatigue.

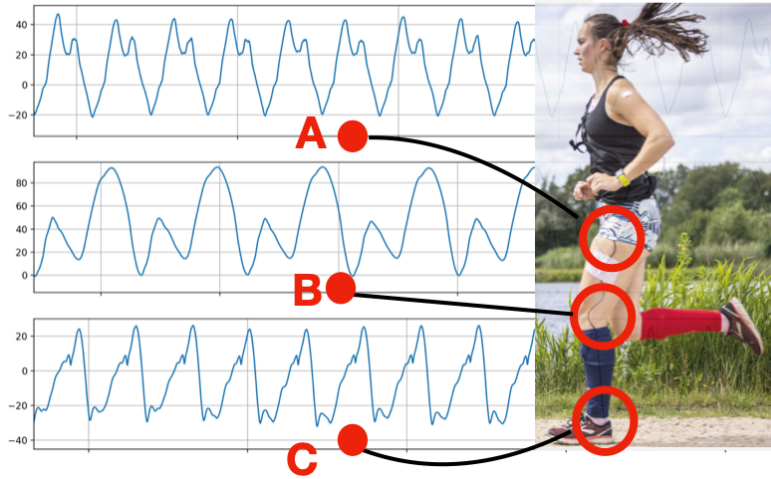


Figure 1: Joint angle patterns for runner³. (A) Hip (B) Knee (C) Ankle angles, over time.

Devices used in data collection are smartwatches tracking the heart rate, IMUs (inertial measurement units) attached to the body of the athletes and multiple cameras and marker systems, tracking the movement of the runner. Additionally, the participants were asked to assess their perceived level of fatigue during the runs on a scale of 1 to 10 (the so-called Borg scale, Borg (1982)), which is particularly valuable as it provides information on the *perceived level of fatigue* and defines a ground truth that we use to benchmark our data analysis. Each data set contains a tremendous amount of information, and we focus here on measurements that are easy to understand for a general audience. We mostly focus on the analysis of data of the lower extremity joint angles, which can be obtained from the measurements of the IMUs. These measurements show the progression of the angles over time, creating repetitive patterns from stride to stride (see Figure 1 for such exemplary patterns and a sketch of the angles measured). For the analysis of the given data, in this paper we will provide statistical methodology based on martingale theory which is (i) particularly well suited to analyze the data at hand, (ii) distribution-free and simple to implement and to adjust to different data types/ channels and a combination thereof, (iii) simple and hence easy to communicate, (iv) applicable in online monitoring contexts, also with limited computational capacities.

Detection of fatigue is clearly related to detecting some form of change in the data, as will be further elaborated in the following sections. Given a precise data and change point model, specialized procedures may outperform the methods presented herein with respect to precision of the estimated change point, but which comes at the cost of points

³Photo courtesy: Rikkert Harink

(ii)-(iv) above as well as the inherent robustness regarding the data distribution and comprehensively capturing a generic form of change (not limited to just changes in mean and variance for example). By means of this approach, in our data example, we focus on questions such as, (a) feature selection in terms of the type of measurements are suited for fatigue detection in general and (b) aggregation of measurements and features from multiple sources to improve detection. Finally, our methods yield the possibility to build personalised *risk profiles* for individual runners summarising the effect of fatigue on the runner.

This paper is structured as follows. We first introduce the basic model assumptions (Section 2), the mathematical preliminaries and theoretical results (both Section 3), where all technical proofs are deferred to the Appendix . The main theorems forming the basis of our methods are in Theorem 1 and Lemma 1, written more concisely in Algorithm 1 and Algorithm 2 applied in the analysis of the sports data presented herein. Further, the methods presented in Section 3 require certain parameters as input, which are chosen based on simulations for different case scenarios. These simulations are conducted in Section 6 and provides us with the required parametric inputs for computations in the application of our methods to the biomechanical sports data. Section 5 is devoted to our data analysis. There, we present all relevant details and our main findings and conclusions, with complementary results presented in the supplement.

2 Basic model assumptions

In this paper, we assume that independent data, $X_i \in \mathcal{X}, i = 1, 2 \dots$ are obtained in a stream, where the endpoint ($i = N$), i.e., the sample size (N) is unknown in advance and \mathcal{X} is some (abstract) sampling space. We wish to set up a sequential hypothesis testing procedure, applicable to data point X_i as soon as it is available (i.e., without waiting for X_{i+1}). In this respect, our test procedure may be closed-ended (when all data points upto $i = N$ are available) or open-ended (full sample not available). Let us assume the following *local test problems* at time points i , with null hypothesis (H_i) and alternative (K_i):

$$H_i : X_i \text{ has property } \mathcal{P} \quad \text{vs.} \quad K_i : X_i \text{ does not have property } \mathcal{P} \quad (1)$$

In our analysis of the movement of running athletes, it is observed that the movement patterns remain stable up to a certain point T_0 in time. More precisely, from time-point $T = 1$ to time-point $T = T_0$, collected movement patterns follow the same average pattern. This corresponds to the data having a (desired) property \mathcal{P} up to point T_0 . After this point in time, which may correspond to the point in time where the runner begins to fatigue, the movement patterns change and gradually deviate progressively from the initial patterns. This corresponds to the data no longer having property \mathcal{P} . Following

this example, we will make the following model assumption

$$X_1, \dots, X_{T_0} \text{ have property } \mathcal{P} \quad X_i, i > T_0 \text{ do not have property } \mathcal{P}. \quad (2)$$

We further assume that a statistical *local level- α test* Φ_i is available for each local hypothesis H_i . The tests Φ_i do not need to be identical. In particular, the tests may look at varying features of the data, which, in our application, may be local peak and trough values of biomechanical knee angles during the course of the run. We also note here that during a long run, a massive amount of data can be produced, not all of which can and needs to be used. Therefore, we are particularly interested in a method that is not memory intensive.

Our approach is as follows. For each measurement X_i , which in our case could be a single cycle from the lower extremity joint angles collected from the knee, hip and ankle; we perform the hypothesis test Φ_i , for test problem (1). Instead of keeping track of all the data, we will only keep track of the number of rejections and store data close to the current point in time (buffering). The number of rejections is monitored over time and the global null hypotheses at time points t , $\mathcal{H}_t := \bigcap_{i=1}^t H_i$, are accepted until the total number of rejections exceeds a certain time-dependent bound. We will provide two different kinds of bounds that can be used for monitoring the number of rejections in our sequential test problem. Both bounds will be based on recent martingale theory (Balsubramani (2014); Balsubramani and Ramdas (2015); Howard et al. (2020)) discussed further in Section 4.

3 Mathematical Preliminaries

Definition 1. (Local test function Φ_i) For the local (i.e., at fixed time points i) null hypotheses defined in Eq. (1), we define the local statistical hypothesis tests Φ_i by

$$\Phi_i : \begin{cases} \mathcal{X} \rightarrow \{0, 1\}, & \text{where } i = 1, 2, \dots \\ X_i \mapsto \Phi_i(X_i) \end{cases}$$

such that it holds that,

$$\mathbb{P}_{H_i}(\Phi_i(X_i) = 1) = \alpha. \quad (3)$$

Definition 2. (Sequential setup) We define the *sequential hypotheses*

$$\mathcal{H}_t = \bigcap_{i=1}^t H_i, \quad \text{and} \quad \mathcal{K}_t = \bigcup_{i=1}^t K_i, \quad (4)$$

and we denote by \mathcal{H}_∞ the *overall null hypothesis*

$$\mathcal{H}_\infty = \bigcap_{j=1}^{\infty} H_j. \quad (5)$$

For given sequential data points $X_i \in \mathcal{X}, i = 1, 2, \dots$; for the test problem with null hypothesis (4) and local level α as in Definition 1, we define the sequential test statistic M_t as

$$M_t = M_t(\alpha) = \sum_{i=1}^t \mathbb{1}\{\Phi_i = 1\} - t\alpha, \quad \forall t \in \mathbb{N}, \quad (6)$$

where each Φ_i is any appropriately defined local level- α test as in Eq. (3) for the local test problem in Eq. (1).

Remark 1. The sequential test statistic Eq. (6) has the following properties:

- (a) The random variables $\mathbb{1}\{\Phi_i = 1\}, i = 1, 2, \dots$ are independent and identically distributed, even though the local tests applied throughout may differ.
- (b) Because of (a), for any fixed $\alpha \in (0, 1)$, M_t is a centered martingale and $M_t + t\alpha \sim \text{Bin}(t, \alpha)$ under the sequential null hypothesis, \mathcal{H}_t in Eq. (4).

In Section 4, we provide two time-uniform critical thresholds Γ_t for M_t in Eq. (6) such that,

$$\mathbb{P}_{\mathcal{H}_\infty} \left(\exists t \geq s_0 : M_t > \Gamma_t \right) \leq \delta, \quad (7)$$

for some initial time $s_0 \geq 1$, and a global level δ for sequentially monitoring our data. The different time-uniform thresholds are applicable uniquely or in combination for different time regimes as well as specific applications, see Algorithm 1 and Algorithm 2.

Notice that our procedure requires the choice of two significance levels $\alpha, \delta \in (0, 1)$. The choice of δ determines the overall significance level of the sequential procedure and controls the occurrence of false positives, i.e., of early or false detections and is therefore naturally chosen to be small. The local level α , on the other hand, can be seen as a parameter that can, in principle, be set to an arbitrary value in $(0, 1)$. Surprisingly perhaps, choosing $\alpha \approx 0.2$ will result in favourable properties, whereas small values of α , such as the standard choice of $\alpha = 0.05$ lead to inferior performance, as will be demonstrated in our simulations Section 6.

3.1 Related literature

Our approach to sequentially monitoring complex data is related to quite a few relevant topics in the statistics literature. While an exhaustive review is infeasible and outside the scope of this work, the following closely related topics and literature are covered along with similarities and differences to this work.

3.1.1 Statistical Process Control

Clearly, there is a close connection of our initial question to the topic of statistical process control (SPC, See, e.g, Montgomery (2020) for a general introduction to the topic or

Qiu (2017) for a general discussion of SPC in the context of big data analysis). In SPC control charts are applied to monitor processes, often in the manufacturing industry, for change that may correspond to a production system being out of control. Our martingale statistic $M_t(\alpha)$, $t = 1, 2, \dots$ can be considered as a type of control chart, where the control limits are provided by the time-uniform bounds Γ_t . However, the performance of a control chart is usually judged in terms of the *run length distribution* and its *average run length* (ARL). Our viewpoint is slightly different: Using time-uniform bounds, we control the overall probability of having a false alarm uniformly in the sense of (7) for the following reason. One main issue in the monitoring of sports data is the typical run length under control required from a control chart. An hour of running provides data of 10,000 or more strides, these are numbers for which typical control charts are not designed. Moreover, the precise detection of change location is not the primary focus as, say, a delay of 100 strides corresponds to less than a minute of running and can still be considered a timely detection, whereas false alarms need to be ruled out. Finally, many frequently used, traditional control charts require strong parametric assumptions such as a normal distribution and cannot handle a change in the quantities that are monitored (Champ and Woodall, 1987; Shewart, 1931; Lowry et al., 1992; Crowder, 1989; Crosier, 1988). While non-parametric methodology based on ranks, order statistics, signs or general quantiles (see, e.g., Bhattacharya and Jr. (1981); Qiu and Hawkins (2001, 2003); Janacek and Meikle (1997); Amin et al. (1995); Chakraborti et al. (2004)) have been proposed in the literature as well, these approaches are not the right fit for our data analysis, as they were all setup following the usual vantage point assumed in process control.

3.1.2 Higher Criticism

In the context of conducting many independent hypothesis tests with the goal of rejecting the joint null hypothesis, various versions of the test statistic,

$$\text{HC}_{\alpha,t} = \frac{M_t(\alpha)}{\sqrt{\alpha(1-\alpha)}},$$

are often referred to as Higher Criticism statistic in Donoho and Jin (2004) and have been proposed in the literature from as early as Brozek and Tiede (1952). The higher criticism statistic is of particular interest in the context of detecting sparse mixtures, ensuring optimality in a certain regime in a variety of different models (see, e.g., Donoho and Jin (2004); Arias-Castro and Ying (2019); Tony Cai et al. (2011) and the references therein). In an applied context, referred to as Sequential-Goodness-of-fit, (Carvajal-Rodriguez et al., 2009) propose to use the higher criticism statistic to identify the number of hypotheses that can be rejected in a multiple testing procedure providing some sort of relaxed multiplicity control compared to strong control of the FWER and the FDR (neither of which are ensured by this method). While related by using the same kind of statistic, a direct comparison to the methodology proposed in this paper is difficult, as the objectives and models imposed are fundamentally different. It should be noted that the higher criticism

statistic is applied to *needle in a haystack* type of problems, i.e., in unordered settings with few but strong signals. While we expect that using the ordered structure in (2) can be explicitly incorporated to improve the accuracy of the detection of change, this will certainly happen at the expense of simplicity of the proposed method and is therefore not pursued further.

3.1.3 Change Point Detection

The literature on change point (CP) detection is vast and a full review is outside the ambit of this work. However, change point detection can be inferred as either detecting abrupt changes in the the data when a certain property changes (Kawahara and Sugiyama, 2009) or an accumulation of change over time due to external situations, example, remote sensing image data (Wen et al., 2021). A branch of CP- detection, known better as CP-estimation, models known changes in data and interprets the nature and plausibility of the estimates of change. The focus in these is where the existence of change is known and the degree and explanation of change is to be ascertained (Hido et al., 2008). Within CP detection, a well known sub-field is curated by CUSUM (cumulative sum)-like techniques. CUSUM methods are designed for an offline application and/or are computationally quite intense. For an introduction to the case of analysing CP retrospectively, an excellent review can be found in (Siegmund and Venkatraman, 1995). For online change detection in mean, there exist moving window change-detection algorithms, where the size of change is to be specified or all possible window sizes are considered, see (Kirch and Weber, 2018) for a survey article, where various CUSUM-detector statistics are considered, namely Page-CUSUM, MOSUM and mMOSUM. Alternatively, Otto and Breitung (2022), consider backward-CUSUM test, extendable to online monitoring scenario after $t > T$. In such cases, asymptotics typically lead to a Wiener process due to a functional central limit theorem. Under various regularity and mixing conditions, quantiles may be approximated by appropriate bootstrap strategies. Further, parameter choices for these methods affect the kind of changes that these algorithms have the most power to detect. Another substantial shortcoming is the prerequisite of having the knowledge of pre-change and post-change mean (in Page-CUSUM). These techniques, therefore, have stringent parametric prerequisites and misspecifications in these models result in unpredictable results and are hard to interpret. A more detailed discussion of these drawbacks is found in (Romano et al., 2021). (Romano et al., 2021) and (Oskiper and Poor, 2002) also serve as a reference for using a CUSUM-detector for online CP- detection, with the latter proposing to construct CUSUM matrices, however again with the assumptions on density functions of the underlying data. The extensive advances by now in CUSUM type detectors may translate to precise CP- estimates, but may not be so relevant in applications which do not demand the most precise estimates of change location but rather require controlling early detection and achieving robustness towards model misspecification while also being computationally less intense. Further, methods herein only require change analysis over any chosen property of the dataset and is applicable to any choice of feature. A prac-

titioner has full freedom in feature selection, relevant for our work in human movement data and is not restricted to traditional monitoring statistics like mean and variance.

3.1.4 Martingale bounds and the law of the iterated logarithm (LIL)

Concentration bounds for martingales that are uniform over finite times were derived in Balsubramani (2014). The bounds presented therein take the form of the LIL upper bound for very large times t and provide CLT-type bound below the LIL-rate for small enough t and thus provide the theoretical basis for our work. The results have been applied in the context of sequential testing in Balsubramani and Ramdas (2015) for two sample mean testing. As we are only interested in monitoring one particular, very simple martingale, we adjust and extend the proofs in (Balsubramani, 2014) to formulate a bound tailored more precisely towards $M_t(\alpha)$. Since the LIL-based bounds obtained in this manner are not valid for small values of t , we use results of (Howard et al., 2020) to derive time-uniform piece-wise linear bounds which can be applied right from the beginning of a monitoring procedure. The bounds can be hybridized to provide sharp bounds over all time regimes.

4 Theoretical results

In this section, we will state two theoretical results which will be the basis for different sequential procedures proposed in this work. In Theorem 1, we provide the time-uniform bound Γ_t^{LIL} based on the law of the iterated logarithm, which is a refined version of a bound derived in Balsubramani (2014). This theorem is applicable only after a stopping time is reached, hereafter denoted by $s_{0,\text{LIL}}$ and is applicable in a (large-) time regime i.e. for $t \geq s_{0,\text{LIL}}$.

Theorem 1. Let, for $\alpha \in (0, 1/2]$, the random variables $\mathbb{1}\{\Phi_i = 1\} \stackrel{\text{i.i.d.}}{\sim} \text{Bin}(1, \alpha)$ and $M_t = M_t(\alpha)$ be as in Eq. (6). For any $\delta \in (0, 1/2]$, any $k \in (0, 1)$, and κ with

$$\kappa \geq \frac{\frac{1}{2} + \frac{1}{20e^8} - 0.4\alpha + \max\{\frac{1}{6e^4} - 0.1\alpha, 0\}}{1 - \alpha} \quad \text{and} \quad s_{0,\text{LIL}} = \left\lceil \frac{e^4(1 + \sqrt{k})^2}{\kappa\alpha(1 - \alpha)} \log\left(\frac{1}{\delta}\right) \right\rceil,$$

it holds with probability at least $1 - \delta$, for all $t \geq s_0$ simultaneously, that

$$M_t \leq \Gamma_t^{\text{LIL}},$$

where

$$\Gamma_t^{\text{LIL}} = \sqrt{\frac{4}{1 - k} \kappa\alpha(1 - \alpha)t \left(2 \log \log \frac{2\kappa\alpha(1 - \alpha)t}{(1 - \sqrt{k})} + \log \frac{2}{\delta \log\left(\frac{1 + \sqrt{k}}{1 - \sqrt{k}}\right)} \right)} \wedge \frac{2\kappa\alpha(1 - \alpha)t}{e^2} \vee 1.$$

The proof of the above theorem is quite technical and therefore deferred to Section 8.2 in the Appendix .

Remark 2. Note that the initial time $s_{0,\text{LIL}}$ in Theorem 1 can easily reach values of 10,000 and more, when (un-)desirable values of the parameters such as small values of κ, α are chosen. As, on the other hand, a small value of κ decreases the bound Γ^{LIL} by a factor of $\sqrt{\kappa}$, whereas too large values render the bound useless in practice. We will, as a compromise, accept a larger starting point $s_{0,\text{LIL}}$ and use another bound for time points $1 \leq t \leq s_{0,\text{LIL}}$ i.e., in time-regimes prior to stopping time $s_{0,\text{LIL}}$.

To this end, Lemma 1 establishes a piece-wise linear function as a time-uniform bound with an initial time $s_{0,\text{Linear}} = 1$.

Lemma 1. Fix $p \in \mathbb{N} \cup \{\infty\}$, $\alpha \in (0, 1)$, $\delta \in (0, 1)$, $\Delta_1, \dots, \Delta_p \in (0, 1)$ such that $\sum_{j=1}^p \Delta_j \leq \delta$. Define further a sequence of time points t_1, \dots, t_p such that $t_1 \leq t_2 \leq \dots \leq t_p$. Set

$$\tau_0 := 2\alpha \log\left(\frac{1}{\Delta_1}\right), \quad (8)$$

$$\tau_j := \sqrt{t_j t_{j+1}} \frac{\sqrt{\log\left(\frac{1}{\Delta_{j+1}}\right)t_{j+1}} - \sqrt{\log\left(\frac{1}{\Delta_j}\right)t_j}}{\sqrt{\log\left(\frac{1}{\Delta_j}\right)t_{j+1}} - \sqrt{\log\left(\frac{1}{\Delta_{j+1}}\right)t_j}}, \quad j = 1, \dots, p. \quad (9)$$

If Δ_j and t_j , $j = 1, \dots, p$ are such that τ_j , $j = 1, \dots, p-1$ satisfies

$$t_1 \leq \tau_1 \leq t_2 \leq \tau_2 \leq \dots \leq \tau_p \leq t_p, \quad (10)$$

and the piece-wise linear function Γ_t^{Linear} is defined by

$$\Gamma_t^{\text{Linear}} = \sum_{j=0}^{p-1} \sqrt{\frac{1}{8} \log\left(\frac{1}{\Delta_j}\right)} \left(\frac{1}{\sqrt{t_j}} t + \sqrt{t_j} \right) \mathbf{1}\{t \in [\tau_j, \tau_{j+1})\}, \quad (11)$$

the following holds

$$\mathbb{P}_{\mathcal{H}_\infty} (\forall t \in \mathbb{N} M_t \leq \Gamma_t^{\text{Linear}}) \geq 1 - \delta. \quad (12)$$

Remark 3. (Properties of Lemma 1)

1. It is clear that using one linear bound in t to monitor the martingale M_t over time provides an undesirable (linear) asymptotic rate in t . Nonetheless, locally, at the time points t_j , we obtain the following bound

$$\Gamma_{t_j}^L = \sqrt{\frac{t_j}{2} \log\left(\frac{1}{\Delta_j}\right)} \quad \text{for } j = 1, \dots, p,$$

i.e., the correct asymptotic behaviour in t , up to a logarithmic factor. Away from the time points t_j , for $p < \infty$, $\Delta_j \equiv \frac{\delta}{2p}$ and $t_{j+1} = t_j + \frac{s_{0,\text{Linear}}}{p}$ for some initial value

$s_{0,\text{Linear}} > 0$, the additional error for $t_j \leq t \leq t_{j+1}$ is bounded from above by the difference

$$\Gamma_{t_{j+1}}^L - \Gamma_{t_j}^L \approx \sqrt{\frac{s_{0,\text{Linear}} \log(\frac{2p}{\delta})}{8pj}},$$

i.e., a moderate deviation, in particular if p and j assume large values. This issue will be discussed in more detail in Section 4.2.

2. Notice that each τ_j defined in (8) reduces to $\tau_j = \sqrt{t_j t_{j+1}}$ if $\Delta_j \equiv \frac{\delta}{2p}$ and (10) is satisfied automatically.

4.1 Monitoring procedures

The bounds presented in Section 4 provide multiple possibilities of defining thresholds for monitoring procedures for the martingale process. We provide two general approaches which can be readily used or adjusted according to information on the problem at hand. To this end, we will put Theorem 1 and Lemma 1 to use and provide two algorithms for sequential analysis in our setting.

Algorithm 1 Sequential testing via LIL bounds

LIL

- 1: **Fix** $\alpha, \delta \in (0, 1)$ and $k \in (0, 1)$
 - 2: $\kappa \leftarrow \frac{\frac{1}{2} + \frac{1}{20e^8} - 0.4\alpha + \max\{\frac{1}{6e^4} - 0.1\alpha, 0\}}{1-\alpha}$
 - 3: $s_{0,\text{LIL}} \leftarrow \left\lceil \frac{e^4(1+\sqrt{k})^2}{\kappa\alpha(1-\alpha)} \log\left(\frac{1}{\delta}\right) \right\rceil$.
 - 4: $\Gamma_t^{\text{LIL}} \leftarrow \sqrt{\frac{4}{1-k} \kappa\alpha(1-\alpha)t \left(2 \log \log \frac{2\kappa\alpha(1-\alpha)t}{(1-\sqrt{k})} + \log \frac{2}{\delta \log(\frac{1+\sqrt{k}}{1-\sqrt{k}})} \right)}$
 - 5: **for** $t = s_{0,\text{LIL}}, s_{0,\text{LIL}} + 1, \dots$ **do**
 - 6: **if** $M_t > \Gamma_t^{\text{LIL}}$ **then**
 - 7: **return** $\widehat{T}_{0,\text{LIL}} = t$
 - 8: **else set** $t = t + 1$
 - 9: **end if**
 - 10: **end for**
-

Algorithm 1 provides a monitoring method for large time points. However, in cases when monitoring the martingale already before point $s_{0,\text{LIL}}$ is desired, a hybrid approach in Algorithm 2 is proposed, which combines the piece-wise linear bound from Lemma 1 and the LIL-bound from Theorem 1. In this approach, the algorithm splits the overall level δ of the sequential procedure equally between early and later times. Before time point $s_{0,\text{LIL}}$, p linear bounds are used whose construction is based on equidistantly spaced time points $\tau_0 = t_1 \leq t_2 \leq \dots \leq t_p = s_{0,\text{LIL}}$.

Algorithm 2 Sequential testing (Hybrid Algorithm)

- 1: **Fix** $\alpha, \delta \in (0, 1)$, $p \in \mathbb{N}$ and $k \in (0, 1)$
 - 2: **Choose** $\Delta_1, \dots, \Delta_p \in (0, 1)$ such that $\sum_{j=1}^p \Delta_j \leq \delta$.
 - 3: $\tau_0 = t_1 \leftarrow 2\alpha \log\left(\frac{1}{\Delta_1}\right)$
 - 4: $\kappa \leftarrow \frac{\frac{1}{2} + \frac{1}{20e^8} - 0.4\alpha + \max\{\frac{1}{6e^4} - 0.1\alpha, 0\}}{1-\alpha}$
 - 5: $s_{0,\text{LIL}} \leftarrow \left\lceil \frac{e^4(1+\sqrt{k})^2}{\kappa\alpha(1-\alpha)} \log\left(\frac{1}{\delta}\right) \right\rceil$.
 - 6: $t_j \leftarrow t_1 + (j-1)/(p-1)(s_0 - t_1)$
 - 7: $\tau_j \leftarrow \sqrt{t_j t_{j+1}} \frac{\sqrt{\log(\frac{1}{\Delta_{j+1}})t_{j+1}} - \sqrt{\log(\frac{1}{\Delta_j})t_j}}{\sqrt{\log(\frac{1}{\Delta_j})t_{j+1}} - \sqrt{\log(\frac{1}{\Delta_{j+1}})t_j}}$, $j = 1, \dots, p-1$.
 - 8: $\Gamma_t^{\text{Linear}} \leftarrow \sqrt{\frac{1}{8} \log\left(\frac{1}{\Delta_j}\right)} \left(\frac{1}{\sqrt{t_j}} t + \sqrt{t_j} \right)$, $t \in [\tau_j, \tau_{j+1})$,
 - 9: $\widehat{T}_{0,\text{hybrid}} \leftarrow 0$
 - 10: **for** $t = t_0, \dots, s_{0,\text{LIL}}$ **do**
 - 11: **if** $M_t > \Gamma_t^{\text{Linear}}$ **then**
 - 12: **return** $\widehat{T}_{0,\text{hybrid}} = t$
 - 13: **else set** $t = t + 1$
 - 14: **end if**
 - 15: **end for**
 - 16: **if** $T_{0,\text{hybrid}} = 0$ **then**
 - 17: $\Gamma_t^{\text{LIL}} \leftarrow \sqrt{\frac{4}{1-k} \kappa \alpha (1-\alpha) t \left(2 \log \log \frac{2\kappa\alpha(1-\alpha)t}{(1-\sqrt{k})} + \log \frac{2}{\delta \log\left(\frac{1+\sqrt{k}}{1-\sqrt{k}}\right)} \right)}$
 - 18: **for** $t = s_{0,\text{LIL}}, s_{0,\text{LIL}} + 1, \dots$ **do**
 - 19: **if** $M_t > \Gamma_t^{\text{LIL}}$ **then**
 - 20: **return** $\widehat{T}_{0,\text{hybrid}} = t$
 - 21: **else set** $t = t + 1$
 - 22: **end if**
 - 23: **end for**
 - 24: **end if**
-

4.2 Properties of the bounds

We will now discuss the properties of the two bounds and provide a comparison. Clearly, the piece-wise linear bounds are sharpest for $\alpha = \frac{1}{2}$, whereas the LIL-bound scales with α . While $\alpha = \frac{1}{2}$ may not be the most obvious choice for the parameter α , the procedures remain valid with (global-) level of the sequential procedures given by δ (and not α). Therefore, in this section, we consider the case of $\alpha = \frac{1}{2}$. To obtain a better understanding of the methods presented here, we will compute each bound at time-points $t_j = j \cdot K$. Then, the bounds are rewritten in the following form:

$$\phi^{-1}(1 - \gamma_j) \sqrt{\alpha(1 - \alpha)t_j}$$

where ϕ denotes the cdf of the standard normal distribution. This allows for a direct comparison to the asymptotic pointwise bound at time point t_i at level δ obtained via the CLT, that is,

$$\phi^{-1}(1 - \delta) \sqrt{\alpha(1 - \alpha)t_j}.$$

At the points t_j , the linear bound is given by

$$\Gamma_{t_i}^{\text{Linear}} = \sqrt{\frac{1}{2}t_i \log\left(\frac{1}{\Delta_i}\right)}.$$

Using Mill's ratio for the normal distribution, we approximate

$$\sqrt{2 \log(1/\Delta_i)} \approx \phi^{-1}\left(1 - \frac{\Delta_i}{\sqrt{2\pi} \sqrt{2 \log(\frac{1}{\Delta_i})}}\right)$$

and find

$$\Gamma_{t_j}^{\text{Linear}} \approx \phi^{-1}\left(1 - \frac{\Delta_j}{\sqrt{2\pi} \sqrt{2 \log(\frac{1}{\Delta_j})}}\right) \sqrt{\frac{1}{4}t_j},$$

i.e., a moderate adjustment of the level for reasonably chosen Δ_j . Setting $\alpha = \frac{1}{2}$, $k = 0.1$ and $\kappa = 1 - k$ yields a relatively moderate starting point of $s_{0,\text{LIL}} = 615$ and a bound

$$\Gamma_t^{\text{LIL}} \leq \sqrt{t\left(2 \log(\log(0.66t)) + \log\left(\frac{3.06}{\delta}\right)\right)}.$$

Using $t_j = j \cdot K$ we find that the LIL bound is of the following form

$$\Gamma_{t_j}^{\text{LIL}} \leq \phi^{-1}\left(1 - \frac{\delta}{C \log(j)^4 \sqrt{\log(\log(j))}}\right) \sqrt{\frac{1}{4}t_j},$$

for a positive constant $C > 0$. Due to the requirement that $\sum_{j=1}^{\infty} \Delta_j \leq \delta$, it is clear that for sufficiently large values of t and hence j , we have

$$\frac{\Delta_j}{\sqrt{2\pi}\sqrt{2\log(\frac{1}{\Delta_j})}} \gg \frac{\delta}{C \log(j)^4 \sqrt{\log(\log(j))}}$$

Therefore, asymptotically, the bound $\Gamma_{t_j}^{\text{LIL}}$ is superior to the linear bound. However as discussed, this only concerns rather large values of t .

5 Case study: Performance analysis of runners

As discussed before, we will focus on the analysis of the performance of athletes during training, in particular in running, which has gained considerable attention in the biomechanical literature in recent years (see, e.g., Saarakkala et al. (2020) for a review on the use of sensor technology in this context). Our analysis provides a step towards our ultimate goal of giving feedback or intervene via a device or application when data is collected, analysed and results are conveyed back in real time. The aim is therefore to detect change in the movement patterns due to fatigue before the runner notices any tiredness. However, a moderate delay in fatigue detection is acceptable.

As is obvious, running entails higher risk of injuries in the lower extremity joints i.e., the hip, knee and ankle joints. Further, it is known that long-distance and long-duration runs are to be associated with injuries due to the fatigue of the runner (Tam et al., 2017) and specifically in the knees (see, (Van Gent et al., 2007), (Nielsen et al., 2012)) and tracking the onset of changes which may lead to such injuries via the joint angles can help to stop or alter training appropriately. It is therefore, of particular interest to study how running kinematics change due to running-induced fatigue (see Apte et al. (2021) and Zandbergen et al. (2023) as well as references therein). This is done by the study of biomechanical data obtained by using inertial measurement units (IMUs), activity trackers like FitBits as well as recorded video data.

For the application of the methods presented here, we focus on the data from running, obtained using a fatigue protocol. In other words, the data collection is designed in such a manner that it is ensured that the athlete taking part in the study will surely but steadily get tired during the course of the run. As discussed before, the fatigue protocol for data collection may be designed in different ways, see (Apte et al., 2021). In our case, the runners were asked for their average speed in an 8 km run and then the speed of the treadmill would be adjusted to 103% of this speed for the indoor run. In an outdoor setting this was slightly more complicated but was achieved by having a cyclist ride a bike parallel to the runner at the required 103% of the average speed of the runner.

Fatigue has different effects on the knee biomechanics of the runner (Harato et al. (2021)). This is because all lower extremity joints, namely, the hip, knee and ankle joints have to somewhat *adjust* to endure the movement even in a fatigued state and therefore

are the joints undergoing maximum change during the course of the run. The movement of these joints are recorded via the joint angles, which are repeated patterns of the form shown in Figure 1. In sections 5.4, 5.5, 5.8, and 5.9 we study these joint angles in detail and apply different versions of the sequential testing methods given in Algorithm 1 and Algorithm 2 for change point detection. To complement this study, we also analyze data from additional sources as follows. In Section 5.6, we look at the ground reaction forces exerted by the foot, obtained from the forceplates embedded in the treadmill. Obviously, this accounts for indoor setting of the run. We only look at the peak values of this data which are effectively recorded when the foot takes off the ground further incorporating the situation of missing values, i.e., when some of these peak values remain undetected due to external factors and the effect this may have on change point detection. Finally, Section 5.7, we look at the contact time of the left and right foot with the ground during the course of the run. The results from the complete analysis is given in Section 5.10.

5.1 Source devices of data

As mentioned before, we obtain this dataset by conducting running trials with fatigue protocol. Devices used in data collection are (i) inertial sensors produced by Xsens (Xsens MVN link sensors, sampling at 240 Hz, see Schepers et al. (2018)) attached to the body of the athletes, and (ii) Force plate data obtained when athletes ran on one belt of a dual-belt treadmill with an integrated three-dimensional (3D) force plate (custom Y-mill, Culemborg, The Netherlands). From the IMUs, one can obtain angles of the hips, knees and ankles (lower extremity joint angles) in 3- dimensions. From a biomechanical point of view, it makes sense to look at the lower extremity joint angles in the sagittal plane (the plane dividing the body into left and right halves). From the forceplates, the ground reaction forces that are associated with the strike and take-off of the foot are obtained. Note further, that for our data collection experiments, both indoor and outdoor, we had 6 healthy male and female runners between the ages of 22 – 39, with no reported prior injuries to the knee joint. Further, the subjects under study in this data analysis are known to have between 1 – 11 years of experience in running. All subjects also reported to be regularly running at least a couple of times between 10 – 60 km per week as their current training patterns.

5.2 Modelling the data

In this section, we model the data on the example of the progression of the joint angles obtained from the runners. Figure 1 shows a few exemplary cycles of such data for each of the three joints (hip, knee and ankle) under consideration. For each run, several thousand of such stride curves, varying around the respective mean curves, are available for each joint. In such biomechanical data, one stride is basically one cycle, or one functional observation, from a functional data set. Therefore, in the following, we implicitly impose a simple functional signal plus noise model to describe the joint angle data mathematically

per stride. Let $Y_i^k(t)$ denote the i -th stride of runner k , $i = 1, \dots, T_k$, $k = 0, \dots, 5$, where

$$Y_i^k = \mu^k(t) + \epsilon_i^k(t) \quad \text{for all } t \in [0, 1] \quad i = 1, \dots, T_k, \quad k = 0, \dots, 5, \quad (13)$$

where $\mu^k(t)$ is the mean function of the k -th runner and $\epsilon_i^k(t)$ are zero mean stochastic process independent of the *true* signal $\mu^k(t)$. Such problems are considered as a pre-processing step, (see Hörmann and Jammoul (2022)). Post-processing, there is a tremendous amount of appealing methods from functional data analysis to apply to such data. Excellent surveys of functional data analysis (FDA) methods are found in (Wang et al., 2016), (Hsing and Eubank, 2015) and (Horváth and Kokoszka, 2012), while a recent advanced work also incorporates the relevant size of the change in the banach space of continuous functions (see Dette et al. (2020)). However, to avoid technicalities and to demonstrate the appealing simplicity of our approach, even for such complex data, we will refrain from pursuing this direction in this example and introduce a simple pipeline for data analysis in the following section, which also works for other data models than (13).

5.3 Typical procedure for the data analysis

To put our monitoring approach to use, we perform the following steps:

(1) Use the first m_1 data points (or prior data/information) to estimate a reference stride profile for each of the joints in a rested state of the runner. (2) Use the subsequent m_2 data points (strides) to compute the distances D_1, \dots, D_{m_2} of each stride to the reference pattern. (We use the L^2 -distance.) (3) From the m_2 computed differences, estimate the $(1 - \alpha)$ -quantile $\hat{q}_{1-\alpha}$, e.g., the median for a choice of $\alpha = 0.5$. (4) Start monitoring afterwards: Set $S_0 := 0$ and for stride i after the initial $m_1 + m_2$ strides:

- Add 0 if $D_{m_2+i} < \hat{q}_{1-\alpha}$: $S_i = S_{i-1}$
- Add 1 else: $S_i = S_{i-1} + 1$

We look for changes in the data using the martingales $M_i(\alpha) = S_i - \alpha i$, using the sequential monitoring scheme provided in Algorithm 2. Note that if not mentioned otherwise, we set local level $\alpha = 0.22$, the global level to $\delta = 0.1$ and $p = 10$ (number of partitions for linear bounds, see Lemma 1) and compute the martingale by taking the $(1 - \alpha)$ -quantile of the initial third of the dataset S_i . Further, since the length of the dataset is not too large, we mostly make use of the linear bounds as a threshold for the monitoring scheme. Finally, to convey our result of fatigue detection, we give the percentage of the run where a -change- in the data is detected. This is because, every runner ran a different length of time, i.e., up to a point in time when they said they could run no more. Presenting the results in percentage of the full run allows us to standardise the comparison between runners. Further, note that in all of the following plots, the x -axis always corresponds to the sequence of strides during the course of the run, unless otherwise stated.

5.4 Analysis 0: Joint angle data (Single runner, pilot study)

As a first proof of concept, in this section we use the hip, knee and ankle joint angles recorded over time during the course of the fatiguing protocol based on a data set that was collected prior to the data analyzed in the following sections and was a part of a pilot study for formalising the protocol of data collection from multiple runners to follow. As shown in Fig. 2 a *profile* of a single runner can be obtained in terms of the martingale statistic from the hip, knee and ankle angles. Further, this is provided along with the point of change given by the upcrossing of the martingale over the linear bounds. We present here the results for $\alpha = 0.22$, which was suggested by our simulations as the most stable parameter choice for which change was detected relatively early, and for $\alpha = 0.05$, the default choice for α . A couple of first interesting results that we find are (a) the martingale statistic of the right ankle angle is significantly different from the rest of the runner profile, as it does not clearly show a steady deviation from the initial reference movement pattern. This may be connected to the known that fatigue impacts the lower joint angles such that increased asymmetry in the load of hip, knee and ankle joints may be seen (see Gao et al. (2022)). (b) The local level α plays a significant role in fatigue detection: As expected, change is detected sooner for $\alpha = 0.22$ and the detected change points within- (i.e., per joint) and between- joints are more consistent in this case with CP at approximately 40% of the run.

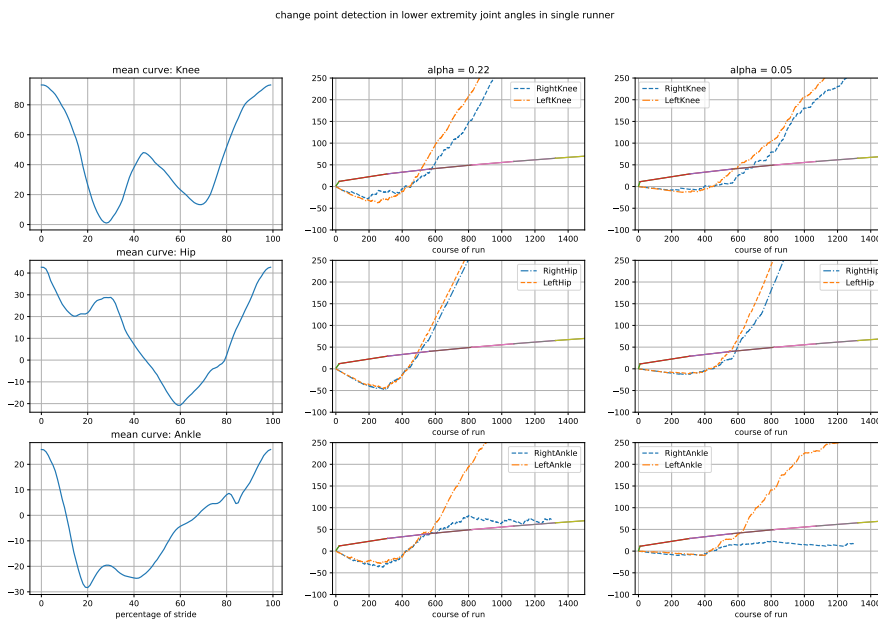


Figure 2: Single runner profile for lower joint angles. Average curves (left col.) and the corresponding martingale statistic for $\alpha = 0.22$ (middle col.) and for $\alpha = 0.05$ (right col.).

Qualitatively, the progression of the martingale trajectories is such that before the

onset of a steep increase indicating change in movement pattern, there is an obvious decrease, indicating a very stable phase preceding the onset of fatigue, which is consistent with biomechanical modelling of typical phases during a fatiguing run. The steep increase on the other hand suggests that fatigue does in fact manifest altered movement patterns and therefore larger deviations from the initial reference pattern. This pattern of the martingale trajectory is also seen and discussed in the following analyses for multiple runners and features other than joint angles.

5.5 Analysis I: Joint angle data (Multiple runners, follow-up study)

A runner profile as in Fig. 2 may be obtained for a group of runners by further applying this methodology across all the runners in both indoor and outdoor settings. This is shown in Fig. 3 and Fig. 9 (for indoors and outdoors) respectively. The percentage of the run where the change is detected by the martingale statistic in both cases is further noted in Table 10 and Table 11 (indoor and outdoor) respectively. Remarkably, we observe for most runners and joint angles the characteristic *check-mark-like form* of the martingale trajectories. For most runners, however, there does appear to be asymmetries per joint. Such individual characteristics of fatiguing are of independent interest in a biomechanical context, as they might be used to provide *personalized feedback* and to create *individualized risk profiles* for a runner paving the way for deeper analyses in case of stark asymmetries.

5.6 Analysis II: Using specific features/ missing data

Using the data from the force plates integrated into the treadmill, we only monitor the peak values at the maximum of each curve. These are the values corresponding to the take-off of the foot during the run. Further we mimic the possibility of missing values in the data. In practise, this would help in case a measurement system does not detect a few signals due to some external influence. In Fig. 4, we use the force plate data from the single runner from the pilot study, shown in Fig. 2. As can be seen, the forceplate data too detects changes at around 40% of the run as seen before in the joint angles. As this data is not available for multiple runners, we only suggest this as a potential application and to point out that the methodology can also be applied to a wide range of other features.

5.7 Analysis III: Contact time of foot

In this section, we analyse the time duration of contact of the left and right foot with the ground during the course of the indoor run. In Fig. 10 of the Appendix , we visualise the data for the left and right foot of the single runner (pilot study) along with the corresponding martingales. In Fig. 5, the analysis for 4 runners is shown. Quantitative analysis for multiple runners is hard due to the fact that data is only available in a laboratory setting for a few runners. Evidently, martingale upcrossing over the bounds is rare.

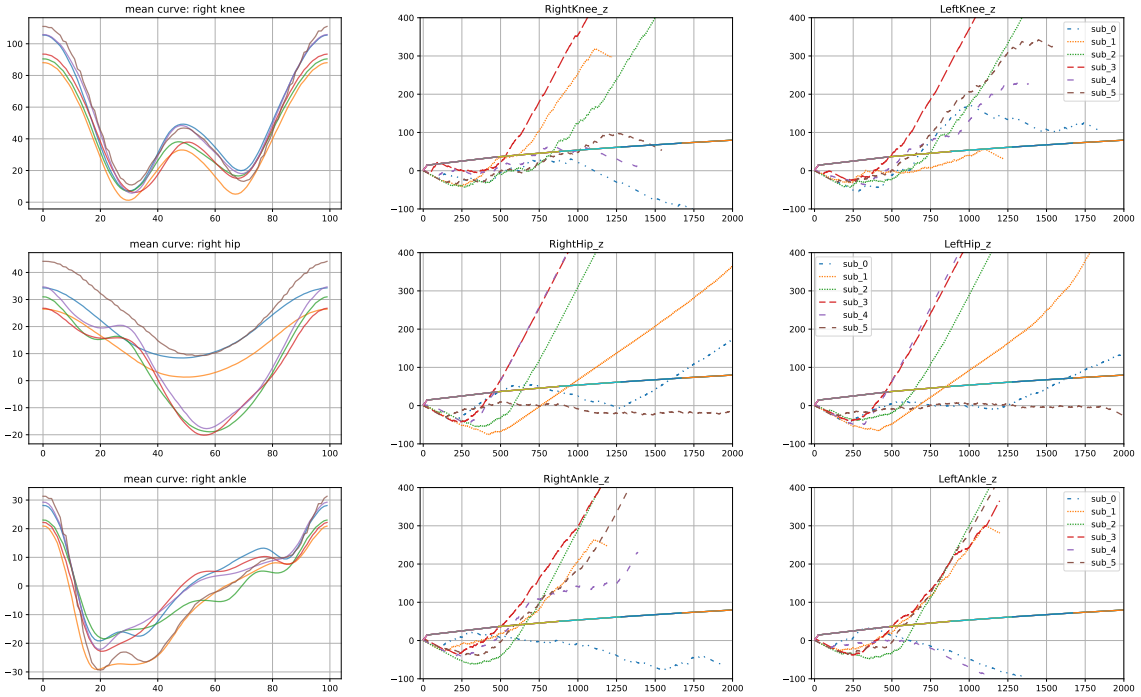


Figure 3: Indoor fatigue profile of all runners. Analysis for local level $\alpha = 0.22$.

However, as before, qualitative analysis shows the sudden onset of a steep increase in all trajectories, reiterating that information on change is contained in the recorded contact times. More clearly than in all the other analyses, we see that initially, an adverse effect plays a role: there seems to be a distinct stable phase before the onset of fatigue, resulting again in *check-mark-shaped* martingale trajectory. In order to capture such a stable phase as well, a segmentation using first a lower martingale bound followed by the given upper bound could be applied resulting in more than one CP, also discussed later in Section 5.10.

Further, current literature also records conflicting results in terms of contact times (a) decreasing during fatigue (Morin et al., 2011) while (b) another study by (Morin et al., 2011) records no changes with (c) (Apte et al., 2021) recording a significant increase. Due to these difficulties, we propose the possibility of this application without further discussion.

5.8 Analysis IV: pooling features from left and right joint angles

In this section we consider aggregated data from left and right joints combined. Using the notation introduced in the box in Section 5.3, we take the distances $D_{ij}^l, D_{ij}^r, i = 1, \dots, m_2, j \in \{\text{hip, knee, ankle}\}$ from the left and the right sides of the body (the latter corresponding to superscripts l, r) and first use $D_j^{\max} = \max\{D_{ij}^l, D_{ij}^r\}$ to construct the martingale at local level α . The result of such a feature selection are shown in corresponding plots in

Force plate data from z-axis

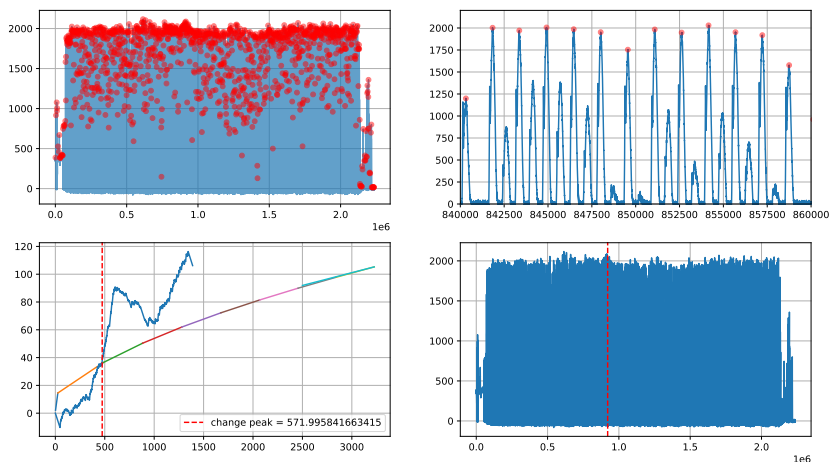


Figure 4: Force plate data. (top left) Data from full run with peaks marked by red dots, (top right) Zoomed in plot, (bottom left) martingale and corresponding bounds, (bottom right) change detected by dashed red line with respect to data from full run.

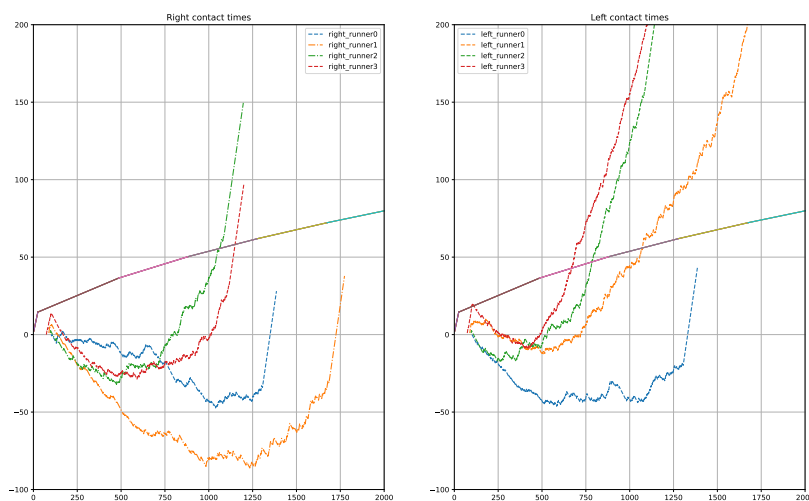


Figure 5: Martingales for contact times of the foot with ground. Visualise data in Fig. 10.

Fig. 6 and the points of up-crossing the bound (in percentages) are provided in Table 12 in the supplement. Similarly to the previous case, we also look at $D_j^{\min} = \min\{D_{ij}^l, D_{ij}^r\}$ and $D_j^{\text{ave}} = \frac{1}{2}(D_{ij}^l + D_{ij}^r)$. Corresponding results are shown in Table 14 and Table 13, respectively. Further, as a comparison, the same is done for outdoor data setting for the

case of D_j^{\max} (see Table 15). An inspection of the tables suggests the use of D_j^{\min} to avoid too early detection due to short instabilities during the run. The maximum and mean produce similar results in general, where D_j^{\max} produces the most stable results in cases where left and right side are unbalanced.

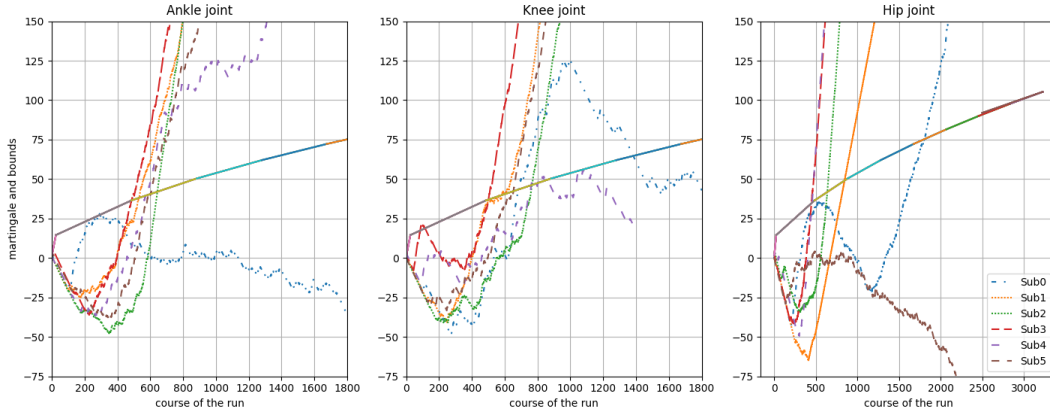


Figure 6: Martingales from pooled data from the left and right sides $\tilde{D}_j^{\max} = \max\{D_{ij}^l, D_{ij}^r\}$.

5.9 Analysis V: Benchmarking with CUSUM and Borg Scale

In order to benchmark our results of detecting fatigue, we use the response of the runner during the course of the run which was taken in the Borg Scale, a scale from 1 to 10, from relaxed to total exhaustion. For a discussion on the Borg scale, see (Borg, 1982). In Table 1, the recorded Borg scale of the runners from our dataset is given. Further, a methodological benchmarking analysis for this particular application was also performed using a CUSUM-like change point detector (see statistic in Eq. (16)), the results of which are in Table 16, Table 17 and Table 18 in the Appendix. It is to be noted that using a CUSUM detector on the sports data, change points appear to be detected either too early or too late. Figure 7 shows a summary of the maximum-pooled values for all angles per subject for the indoors data alongwith Borg scale values. It can be seen that up to at least a reported/*perceived* level of fatigue of 4 (the transition from light activity to moderate activity) a stable phase can be consistently observed for all the runners. Furthermore, change is typically detected while moving from moderate to vigorous activity (the latter starting at 7). Therefore, we conclude that the martingale trajectory captures the progression of the perceived level of fatigue consistently.

5.10 Conclusion

In this section, we summarize the main findings of our case study and provide ideas for future research. A first conclusion to be reached from Analysis 0 is that for well-processed

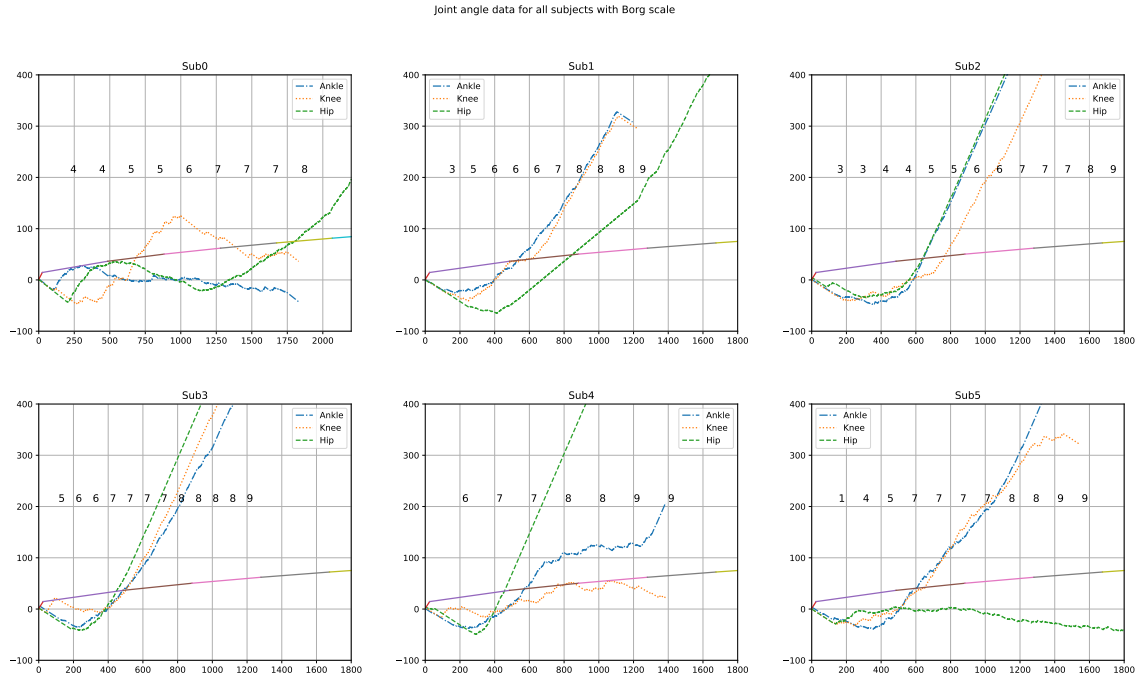


Figure 7: Joint angle data analysis (pooled for the left and right sides and taking max as in Section 5.8) from indoor per subject with the corresponding Borg scales.

% of run	Indoor						Outdoor					
	Subject 0	Subject 1	Subject 2	Subject 3	Subject 4	Subject 5	Subject 0	Subject 1	Subject 2	Subject 3	Subject 4	Subject 5
0.0	1	2	1	1	2	1	1	2	1	1	1	1
25.0	4	5	3	6	7	7	4	5	3	4	4	7
50.0	6	6	6	7	8	7	6	7	6	7	6	8
75.0	7	8	7	8	8	9	7	8	8	7	7	9
100.0	8	9	9	9	9	10	8	9	10	9	8	10

Table 1: Reported Borg scales of all subjects, indoor and outdoor corresponding to percent of run.

data measured in a controlled (indoor) environment, results are extremely stable and change points are detected consistently at the same point throughout features (see Figure 2). This is even the case if much noisier data is used for the analysis (Analysis II, Figure 4). Further, it is also observed that a (local-)level of $\alpha = 0.22$ produces good results simultaneously for all data, especially joint angle and forceplate, even in non-standard situations like missing data, studied in Section 5.6.

Further, as seen in the case of aggregated data in Fig. 6 (corresponding CPs reported in Table 12 in the supplement), CP-detection is seen to have certain alignment within the joint angles, especially in the case of ankle and hip joint. Qualitatively, the deviations, for example, in the case of Subject 0 (ankle); Subject 0 and Subject 4 (knee), the statistic is seen to stabilize with respect to the null hypothesis.

It is to be also noted that even though upcrossing of the martingale may not always take place (see Fig. 5), the martingale process contains information in its trajectory, which can be used to analyze a run retrospectively. In this context, it is worth mentioning that the trajectories of all the runners suggest a certain stability and then show a steady increase (with CP at around 40% of the run) from which an inference can be made that most local tests at these (later) time-points were rejected. We remark that qualitative information can be deciphered from the use of the sequential martingale statistic, yielding the positions of increase, where it follows that incoming data are progressing deviating from the reference.

Further, as a proof of concept for the use of joint angle data for the purpose of fatigue detection, from Figures 3 and 9 it can be safely concluded that all runners have at least one joint suitable for this task. This is supplemented in Fig. 7 with a subject wise analysis benchmarked by the corresponding Borg scale (indoor data), showing that the behaviour of the martingale trajectory is in line with the reported (*perceived*) level of fatigue.

When monitoring joint angles, our analysis showed a strong variability in symmetry within individuals, which can be reduced by a combination of different features in cases where the main focus is on fatigue detection. For simplicity and proof of concept, in this study we only considered aggregation of left and right joints, as these are automatically on the same scale. However, aggregation of a larger number of features promises even better results, but needs to be carefully designed and studied, potentially in future research. Our data analysis shows that the use of the martingale statistic is well suited for the analysis of such data. Future research and extension towards a quantitative analysis of the whole martingale trajectory along-with the development of an adjusted procedure incorporating a lower bound of the martingale (follows due to symmetry), is foreseen to be advantageous in multiple change detection. In our example, this would be particularly beneficial for the definition of different phases in a run with respect to levels of fatigue. From an application point of view, such a refined approach would allow a practitioner to track subtle changes, where even slight departures from reference movements during the course of the activity are monitored. This is expected to be particularly helpful in human movement analysis not just in fatigue detection and injury prevention but also in rehabilitation.

Ethics statement: The local ethics committee (Ethical Committee EEMCS (EC-CIS), University of Twente, ref.: RP 2022-20) approved the experimental protocol of this study.

Acknowledgements: The author thanks RUB for their hospitality where a part of the research was carried out. Both authors thank all members of the *Sports, Data, and Interaction project*, in particular Dennis Reidsma and Jasper Reenalda, for helpful discussions and valuable feedback. Further, the authors report there are no competing interests to declare.

References

- Amin, R. W., Jr., M. R. R., and Saad, B. (1995). Nonparametric quality control charts based on the sign statistic. *Communications in Statistics-Theory and Methods*, 24(6):1597–1623.
- Apte, S., Prigent, G., Stöggl, T., Martínez, A., Snyder, C., Gremeaux-Bader, V., and Aminian, K. (2021). Biomechanical response of the lower extremity to running-induced acute fatigue: a systematic review. *Frontiers in physiology*, 12:646042.
- Arias-Castro, E. and Ying, A. (2019). Detection of sparse mixtures: higher criticism and scan statistic. *Electronic Journal of Statistics*, 13(1):208 – 230.
- Balsubramani, A. (2014). Sharp finite-time iterated-logarithm martingale concentration. *arXiv preprint arXiv:1405.2639*.
- Balsubramani, A. and Ramdas, A. (2015). Sequential nonparametric testing with the law of the iterated logarithm.
- Bhattacharya, P. K. and Jr., D. F. (1981). A Nonparametric Control Chart for Detecting Small Disorders. *The Annals of Statistics*, 9(3):544 – 554.
- Borg, G. A. (1982). Psychophysical bases of perceived exertion. *Medicine & science in sports & exercise*.
- Brozek, J. and Tiede, K. (1952). Reliable and questionable significance in a series of statistical tests. *Psychological Bulletin*, 49:339–341.
- Buist, I., Bredeweg, S. W., Lemmink, K. A. P. M., van Mechelen, W., and Diercks, R. L. (2010). Predictors of running-related injuries in novice runners enrolled in a systematic training program: A prospective cohort study. *The American Journal of Sports Medicine*, 38(2):273–280.
- Carvajal-Rodriguez, A., de Una-Alvarez, J., and Rolan-Alvarez, E. (2009). A new multitest correction (sgof) that increases its statistical power when increasing the number of tests. *BMC Bioinformatics*, 10:209.
- Chakraborti, S., Van der Laan, P., and Van de Wiel, M. (2004). A class of distribution-free control charts. *Journal of the Royal Statistical Society: Series C (Applied Statistics)*, 53(3):443–462.
- Champ, C. W. and Woodall, W. H. (1987). Exact results for shewhart control charts with supplementary runs rules. *Technometrics*, 29(4):393–399.
- Crosier, R. B. (1988). Multivariate generalizations of cumulative sum quality-control schemes. *Technometrics*, 30(3):291–303.
- Crowder, S. V. (1989). Design of exponentially weighted moving average schemes. *Journal of Quality technology*, 21(3):155–162.
- Dette, H., Kokot, K., and Aue, A. (2020). Functional data analysis in the banach space of continuous functions.
- Donoho, D. and Jin, J. (2004). Higher criticism for detecting sparse heterogeneous mixtures. *The Annals of Statistics*, 32(3):962 – 994.

- Gao, Z., Fekete, G., Baker, J. S., Liang, M., Xuan, R., and Gu, Y. (2022). Effects of running fatigue on lower extremity symmetry among amateur runners: From a biomechanical perspective. *Frontiers in Physiology*, page 1792.
- Harato, K., Morishige, Y., Niki, Y., Kobayashi, S., and Nagura, T. (2021). Fatigue and recovery have different effects on knee biomechanics of drop vertical jump between female collegiate and recreational athletes. *Journal of Orthopaedic Surgery and Research*, 16:1–7.
- Hido, S., Idé, T., Kashima, H., Kubo, H., and Matsuzawa, H. (2008). Unsupervised change analysis using supervised learning. In *Advances in Knowledge Discovery and Data Mining: 12th Pacific-Asia Conference, PAKDD 2008 Osaka, Japan, May 20-23, 2008 Proceedings 12*, pages 148–159. Springer.
- Hörmann, S. and Jammoul, F. (2022). Consistently recovering the signal from noisy functional data. *Journal of Multivariate Analysis*, 189:104886.
- Horváth, L. and Kokoszka, P. (2012). *Inference for functional data with applications*, volume 200. Springer Science & Business Media.
- Howard, S. R., Ramdas, A., McAuliffe, J., and Sekhon, J. (2020). Time-uniform chernoff bounds via nonnegative supermartingales. *Probability Surveys*, 17:257–317.
- Hsing, T. and Eubank, R. (2015). *Theoretical foundations of functional data analysis, with an introduction to linear operators*, volume 997. John Wiley & Sons.
- Janacek, G. and Meikle, S. (1997). Control charts based on medians. *Journal of the Royal Statistical Society: Series D (The Statistician)*, 46(1):19–31.
- Kawahara, Y. and Sugiyama, M. (2009). Change-point detection in time-series data by direct density-ratio estimation. In *Proceedings of the 2009 SIAM international conference on data mining*, pages 389–400. SIAM.
- Kirch, C. and Weber, S. (2018). Modified sequential change point procedures based on estimating functions. *Electronic Journal of Statistics*, 12:1579–1613.
- Lowry, C. A., Woodall, W. H., Champ, C. W., and Rigdon, S. E. (1992). A multivariate exponentially weighted moving average control chart. *Technometrics*, 34(1):46–53.
- Lu, T.-W. and Chang, C.-F. (2012). Biomechanics of human movement and its clinical applications. *The Kaohsiung journal of medical sciences*, 28:S13–S25.
- Montgomery, D. C. (2020). *Introduction to statistical quality control*. John Wiley & Sons.
- Morin, J.-B., Samozino, P., and Millet, G. Y. (2011). Changes in running kinematics, kinetics, and spring-mass behavior over a 24-h run. *Medicine & Science in Sports & Exercise*, 43(5):829–836.
- Nielsen, R., Buist, I., Sørensen, H., Lind, M., and Rasmussen, S. (2012). Training errors and running related injuries: a systematic review. *Int J Sports Phys Ther.*, 7(9):58–75.
- Oskiper, T. and Poor, H. V. (2002). Online activity detection in a multiuser environment using the matrix cusum algorithm. *IEEE Transactions on Information Theory*, 48(2):477–493.
- Otto, S. and Breitung, J. (2022). Backward cusum for testing and monitoring structural change with an application to covid-19 pandemic data. *Econometric Theory*, pages 1–34.

- Postema, K., Hermens, H. J., De Vries, J., Koopman, H. F., and Eisma, W. (1997). Energy storage and release of prosthetic feet part 1: Biomechanical analysis related to user benefits. *Prosthetics and Orthotics International*, 21(1):17–27.
- Qiu, P. (2017). Statistical process control charts as a tool for analyzing big data. *Big and Complex Data Analysis: Methodologies and Applications*, pages 123–138.
- Qiu, P. and Hawkins, D. (2001). A rank-based multivariate cusum procedure. *Technometrics*, 43(2):120–132.
- Qiu, P. and Hawkins, D. (2003). A nonparametric multivariate cumulative sum procedure for detecting shifts in all directions. *Journal of the Royal Statistical Society: Series D (The Statistician)*, 52(2):151–164.
- Robbins, H. and Siegmund, D. (1970). Boundary crossing probabilities for the wiener process and sample sums. *The Annals of Mathematical Statistics*, pages 1410–1429.
- Romano, G., Eckley, I., Fearnhead, P., and Rigall, G. (2021). Fast online changepoint detection via functional pruning cusum statistics. *arXiv preprint arXiv:2110.08205*.
- Saarakkala, S., Taborri, J., Keogh, J., Kos, A., Santuz, A., Santuz, A., Umek, A., Urbanczyk, C., van der Kruk, E., and Rossi, S. (2020). Sport biomechanics applications using inertial, force, and emg sensors: A literature overview. *Applied Bionics and Biomechanics*, 2020:18 pages. Article ID 2041549.
- Scheerder, J., Breedveld, K., and Borgers, J. (2015). Who Is Doing a Run with the Running Boom? In *Running across Europe: The Rise and Size of One of the Largest Sport Markets*, pages 1–27. Palgrave Macmillan UK, London.
- Schepers, M., Giuberti, M., Bellusci, G., et al. (2018). Xsens mvn: Consistent tracking of human motion using inertial sensing. *Xsens Technol*, 1(8).
- Shafer, G. and Vovk, V. (2005). *Probability and finance: it's only a game!*, volume 491. John Wiley & Sons.
- Shewart, W. (1931). Economic control of quality of manufactured product. *Bull. Amer. Soc. Qual. Control*.
- Siegmund, D. and Venkatraman, E. (1995). Using the generalized likelihood ratio statistic for sequential detection of a change-point. *The Annals of Statistics*, pages 255–271.
- Tam, N., Coetzee, D. R., Ahmed, S., Lamberts, R. P., Albertus-Kajee, Y., and Tucker, R. (2017). Acute fatigue negatively affects risk factors for injury in trained but not well-trained habitually shod runners when running barefoot. *European Journal of Sport Science*, 17(9):1220–1229.
- Tony Cai, T., Jessie Jeng, X., and Jin, J. (2011). Optimal Detection of Heterogeneous and Heteroscedastic Mixtures. *Journal of the Royal Statistical Society Series B: Statistical Methodology*, 73(5):629–662.
- Van Gent, R., Siem, D., van Middelkoop, M., Van Os, A., Bierma-Zeinstra, S., and Koes, B. (2007). Incidence and determinants of lower extremity running injuries in long distance runners: a systematic review. *British journal of sports medicine*, 41(8):469–480.
- Wang, J.-L., Chiou, J.-M., and Müller, H.-G. (2016). Functional data analysis. *Annual Review of Statistics and its application*, 3:257–295.

- Wen, D., Huang, X., Bovolo, F., Li, J., Ke, X., Zhang, A., and Benediktsson, J. A. (2021). Change detection from very-high-spatial-resolution optical remote sensing images: Methods, applications, and future directions. *IEEE Geoscience and Remote Sensing Magazine*, 9(4):68–101.
- Yoshioka, S., Nagano, A., Hay, D. C., and Fukashiro, S. (2009). Biomechanical analysis of the relation between movement time and joint moment development during a sit-to-stand task. *Biomedical engineering online*, 8(1):1–9.
- Zandbergen, M. A., Marotta, L., Bulthuis, R., Buurke, J. H., Veltink, P. H., and Reenalda, J. (2023). Effects of level running-induced fatigue on running kinematics: A systematic review and meta-analysis. *Gait & Posture*, 99:60–75.
- Zandbergen, M. A., Reenalda, J., van Middelaar, R. P., Ferla, R. I., Buurke, J. H., and Veltink, P. H. (2022). Drift-free 3d orientation and displacement estimation for quasi-cyclical movements using one inertial measurement unit: Application to running. *Sensors*, 22(3):956.

Appendix

This section of the manuscript consists of all the simulations and the results therein in Section 6. This includes the change-point detection in various scenarios and the comparison of the methods presented in this manuscript with a standard CUSUM- detector statistic. This is followed by the Section 7 which consists of all the figures and tables from the main part of the manuscript, comprising of the results of the data analysis. Finally the proofs of Theorem 1 and Lemma 1 are provided in Section 8.

6 Simulations

In this section, we evaluate our methods on simulated data. This is done in two settings to understand (1) the qualitative estimation of the change point with respect to the true change point in various combinations of distributions and (2) the impact of the local-level α and global-level δ in the sequential testing scenario and finally (3) a comparison in change point detection with respect to a standard CUSUM-like detector statistic. The mathematical model for the simulated data is as follows. We choose a sequence of points $X_1, X_2, \dots, X_n \in \mathbb{R}$ such that an underlying model ensures exactly one *true* change point. A martingale is then constructed such that,

$$M_t = \sum_{i=1}^t \mathbb{1}\{X_i > \gamma_{1-\alpha}\} - t\alpha, \quad (14)$$

where α and $\gamma_{1-\alpha}$ are such that $P(X_i > \gamma_{1-\alpha}) = \alpha$ before the change point and $P(X_i > \gamma_{1-\alpha}) > \alpha$ after the change point. In what follows, $\gamma_{1-\alpha}$ is the estimated $(1 - \alpha) \times 100\%$ -quantile from the first 10% of data points in the sequence X_i , as described in the box in Section 5.3. Naturally, this is only possible in a retrospective setting, at least until the required initial fraction of the data is available. In a sequential setting, an appropriate choice of γ_α can be done on prior data or based on a pre-determined number of initial data points. Further, the martingale bounds are then constructed with this choice of α along with the other essential parameters.

6.1 Change point detection in different scenarios

In this section, we explore the abilities of our martingale statistic as a change point detector in dependence on the parameter α . To this end, we choose simple models following distributions where it gets increasingly harder to detect the change point i.e.,

$$Y_{ij} = \chi_{k_j}^2, \quad i = 1, \dots, n, \quad j = 1, \dots, 4, \quad (15)$$

where the index i denotes the samples drawn from a χ^2 -distribution with k_j -degrees of freedom in different scenarios numbered by the index j . A visual representation of the simulated data is provided in Fig. 8, where j varies along the left panels from top to bottom

with increasing level of difficulty and i corresponds to the x -axis of each panel i.e., the stream of data under study. Note that the fatigue protocol is designed to induce fatigue rather quickly and thus generates relatively short data streams. Here, we simulated longer data streams as compared to our data sets to evaluate the feasibility of the procedure in more realistic training settings. We work with the situation where the true change point lies at the location $i = \frac{n}{2}$ and $j = 1, \dots, 4$. When this is not the case, it is explicitly mentioned. The degrees of freedom for χ^2_{kj} for each j are given in Table 2. Using this setting, we now compute martingale bounds for $\alpha \in \{0.05, 0.25, 0.5\}$ and discuss the change point detection results in Tables 3-5, for the different local-levels α respectively. We chose a simple change point model to provide a general proof of concept. The χ^2 -distribution was chosen as, in the case of the analysis of the joint angle data, we expect the the observed L^2 -distances to follow χ^2 -type distributions. However, in contrast to model (15) the real data typically show a more complicated behaviour of gradual and multiple changes and the presence of outliers, which is easily handled by our martingale approach, but more challenging for standard change point detection strategies.

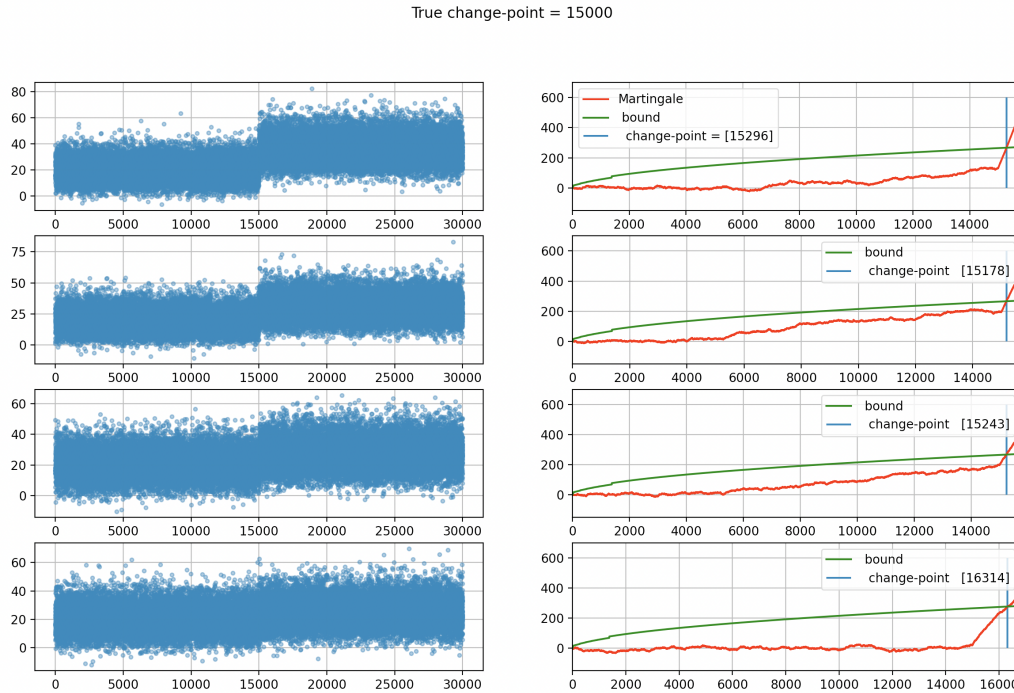


Figure 8: Left: Exemplary simulated data following model (15) with increasing level of difficulty from top to bottom (for the exact degrees of freedom of the χ^2 -distributions see Table 2). Left: Corresponding martingale and bounds and exemplary martingale trajectories of the martingales (14).

panel number	degrees of freedom (before cp)	degrees of freedom (after cp)
$j = 1$	20	36
$j = 2$	20	30
$j = 3$	20	27
$j = 4$	20	25

Table 2: Setting for running simulations, making change point detection increasingly harder by bringing degrees of freedom of the χ^2 distributions closer to each other. (See Fig. 8 for four exemplary data sets and corresponding martingale trajectories).

$\alpha = 0.5, \delta = 0.1$	True CP	Est. CP	std dev.	std dev*	Number false positive
$j = 1$	15000	15556.598	800.347	230.683	149
$j = 2$	15000	15632.6317	812.636	261.8841	150
$j = 3$	15000	15769.035	869.8	327.269	142
$j = 4$	15000	15999.196	991.52	428.065	169

Table 3: Estimated average change points, standard deviations and number of false positives for $\alpha = 0.5$ and $\delta = 0.1$ based on 10000 simulation runs for $j = 1$ (easiest) and $j = 4$ (hardest) (see Table 2 for the exact parameter settings).

6.1.1 Discussion : Result analysis

As mentioned before change point detection is harder as we go from panel $j = 1$ to $j = 4$. Therefore it also makes sense that the (mean-) change point detection (along-with observed standard deviations,) makes better estimates for panel $j = 1$ as compared to $j = 4$. Further, observing the results for the (local-) level α , it is seen that a small-local level $\alpha = 0.05$ produces somewhat acceptable estimates for change points only in the most obvious case of $j = 1$, albeit with a large number of false positives (see Table 5) compared to larger values of α . change point estimates for $j = 4$, the case where change point is harder to detect and the situation we are most interested in; are best for $\alpha = 0.25, 0.5$. In the latter case, the observed standard deviation in the estimated change point location is quite high (possibly due to some very early false detections) while the overall number of false positives is relatively lower. When compared to the case of $\alpha = 0.25$ a slightly better performance in terms of the standard deviations can be observed. The choice of the local level is therefore narrowed down to the range $\alpha \in (0.2, 0.5)$. In order to find an optimal value for change point detection, especially in the case of subtle change as in $j = 4$, we pursue simulations with focus on a grid of local levels $\alpha \in [0.2, 0.5]$ and present the results in Table 6. We notice that in terms of having the least number of false positives, the values $\alpha = 0.25, 0.3, 0.5$ work the best. When considered together with the quality of the change point estimation, it appears only the first two are best performing for the (most interesting-) case $j = 4$.

$\alpha = 0.25, \delta = 0.1$	True CP	Est. CP	std dev.	std dev*	Number false positive
$j = 1$	15000	15332.092	528.614	139.63	185
$j = 2$	15000	15439.279	566.91	187.589	185
$j = 3$	15000	15595.733	566.919	263.598	198
$j = 4$	15000	15850.357	738.53	381.25	178

Table 4: Estimated average change points, standard deviations and number of false positives for $\alpha = 0.25$ and $\delta = 0.1$ based on 10000 simulation runs for $j = 1$ (easiest) and $j = 4$ (hardest) (see Table 2 for the exact parameter settings).

$\alpha = 0.05, \delta = 0.1$	True CP	Est. CP	std. dev.	std. dev*	Number false positive
$j = 1$	15000	15175.351	650.412	77.481	249
$j = 2$	15000	15327.588	646.26	154.4	244
$j = 3$	15000	15565.188	708.175	269.389	268
$j = 4$	15000	15930.514	849.81	462.32	246

Table 5: Estimated average change points, standard deviations and number of false positives for $\alpha = 0.05$ and $\delta = 0.1$ based on 10000 simulation runs for $j = 1$ (easiest) and $j = 4$ (hardest) (see Table 2 for the exact parameter settings).Table 2.

6.2 Comparison to CUSUM detector

In this section, the objective is to compare change point detection via our methods as compared to a standard CUSUM statistic. We assume again that Y_{ij} , $i = 1, \dots, n$, $j = 1, \dots, 4$, are independent samples with the underlying model as in Eq. (15) for $j = 4$. A typical CUSUM statistic is given by,

$$\tilde{Y}_t = \sqrt{\frac{(s_2 - t)(t - s_1)}{s_2 - s_1}} (\hat{\mu}_1 - \hat{\mu}_2); \quad s_1 < s_2 - 1 \quad \text{and} \quad t = s_1 + 1, \dots, s_2 - 1, \quad (16)$$

where $\hat{\mu}_1 = \frac{1}{t - s_1} \sum_{i=s_1+1}^t X_i$ and $\hat{\mu}_2 = \frac{1}{s_2 - t} \sum_{i=t+1}^{s_2} X_i$. More specifically, the statistic \tilde{Y}_t scans through time $t \in (s_1, s_2)$ and checks for the maximum deviation in means before and after a (scanning-) time point t . Further, the estimated change point is given by,

$$t_{cp} = \underset{t}{\operatorname{argmax}} |\tilde{Y}_t|. \quad (17)$$

In this way, the time point showing maximum deviation to the mean before and after it is considered the time point of change. Results of the analysis are presented in Tables 7-9, where the underlying model has a change point at an initial part, at the mid-point and towards the end respectively. As reflected in the precise estimation results of the CUSUM detector, our model provides a very simple task for such classical approaches. In more realistic situations where change sets in gradually, multiple change points as well

	local-, global-, level	True CP	Est. CP	std. dev	std. dev*	Number false positive
	$\alpha = 0.2$	15000	15845.278	920	384.462	317
	$\alpha = 0.22$	15000	15850.392	467.875	358.826	163
	$\alpha = 0.25, \delta = 0.1$	15000	15832	466.671	372.87	66
	$\alpha = 0.3, \delta = 0.1$	15000	15850.993	554.145	363.214	91
	$\alpha = 0.36, \delta = 0.1$	15000	15895	1027.735	382.822	159
	$\alpha = 0.45, \delta = 0.1$	15000	15916	811.16	416.933	134
	$\alpha = 0.5, \delta = 0.1$	15000	16004	808.657	443.6289	69

Table 6: Narrowing down the choice of α : Estimated average change points, standard deviations and number of false positives for α between 0.2 and 0.5 and $\delta = 0.1$ based on 10000 simulation runs for the scenario given in $j = 4$ i.e., situations where the change point is hardest to detect.

(local-) (global-) level	True CP	CUSUM	Martingale CP (mean)	overall std	std*	false positives
$\alpha = 0.25, \delta = 0.1$	5000	5000.1484	5121.9596	25.07376 2538	-	0
$\alpha = 0.1, \delta = 0.1$	5000	5000.1498	5121.1066	22.97	-	0
$\alpha = 0.5, \delta = 0.1$	5000	5000.14	5127.3645	38.65057360	-	0

Table 7: Comparison to standard CUSUM statistic based on 10000 simulations of scenario $j = 4$, where the true CP lies at an initial part of a sequence of in total 30000 data points for different values of α and $\delta = 0.1$.

as outliers may be present, such methods are certainly more deeply affected than our martingale approach. Since this becomes evident in the comparison of the performances of both approaches in our data analysis, we refrain from investigating this issue further in our simulations.

Despite that, it is important to note the following, (a) Scan-statistic: this means computations are repeated over the scanning index t . This results in the CUSUM being more memory intensive as already discussed in Section 4.2. (b) While online variations of the CUSUM-detector exist, it is important to note that our method only makes minimal assumptions on the underlying model and distribution of the data which is a clear advantage over CUSUM (see again, Section 4.2). (c) Finally, we note that our data analysis does not focus on recovering precise change points but rather on robust, widely applicable sequential analysis of CP-detection while controlling an overall error of false alarms, i.e. early detection. In order to provide a more complete picture, Tables 7- 9, in addition to the sample standard deviation (std dev) of the estimated change point location, we also list the standard deviation after removing the false positives (std dev*).

(local-) (global-) level	True CP	CUSUM	Martingale CP (mean)	overall std	std*	false positives
$\alpha = 0.25, \delta = 0.1$	15000	15000.1626	15467.4207	954.0 1	225.934	148
$\alpha = 0.1, \delta = 0.1$	15000	15000.1432	15459.1764	864.26	236.69	148
$\alpha = 0.5, \delta = 0.1$	15000	15000.1432	15477.0819	876.81	228.02	163

Table 8: Comparison to standard CUSUM statistic based on 10000 simulations of scenario $j = 4$, where the true CP lies in the middle of a sequence of in total 30000 data points for different values of α and $\delta = 0.1$.

(local-) (global-) level	True CP	CUSUM	Martingale CP (mean)	overall std	std dev*	false positives
$\alpha = 0.25, \delta = 0.1$	25000	25000.1659	24781.1254	2279. 1626	157.053089	678
$\alpha = 0.1, \delta = 0.1$	25000	25000.1454	24745.155	2393.28	153.81	691
$\alpha = 0.5, \delta = 0.1$	25000	25000.136	24783.6333	2265.55	169.579	687

Table 9: Comparison to standard CUSUM statistic based on 10000 simulations of scenario $j = 4$, where the true CP lies at 5/6 of a sequence of in total 30000 data points for different values of α and $\delta = 0.1$.

7 Figures and tables from Section 5

Note that in Section 5, only a selection of figures and tables were given to underline our main findings. For the sake of completeness, we now present the figures (Fig. 9, Fig. 10) and tables (Table 12-Table 15; nan- values correspond to no upcrossing of the martingale on the bounds) that were left out in the main document.

	subject 0	subject 1	subject 2	subject 3	subject 4	subject 5
Right Knee	nan	56.628	48.422	47.456	0.0	74.11
Left Knee	38.113	nan	44.924	46.218	48.348	44.293
Right Hip	10.932	42.296	37.056	41.376	38.982	nan
Left Hip	56.419	43.769	38.847	41.66	38.217	nan
Right Ankle	10.859	60.132	38.168	45.765	43.359	40.915
Left Ankle	15.45,	52.059	37.157	48.316	nan	39.857

Table 10: Data from lower extremity joint angles in indoor setting. Percentage of the run where an up-crossing of the martingale is seen for all the runners.

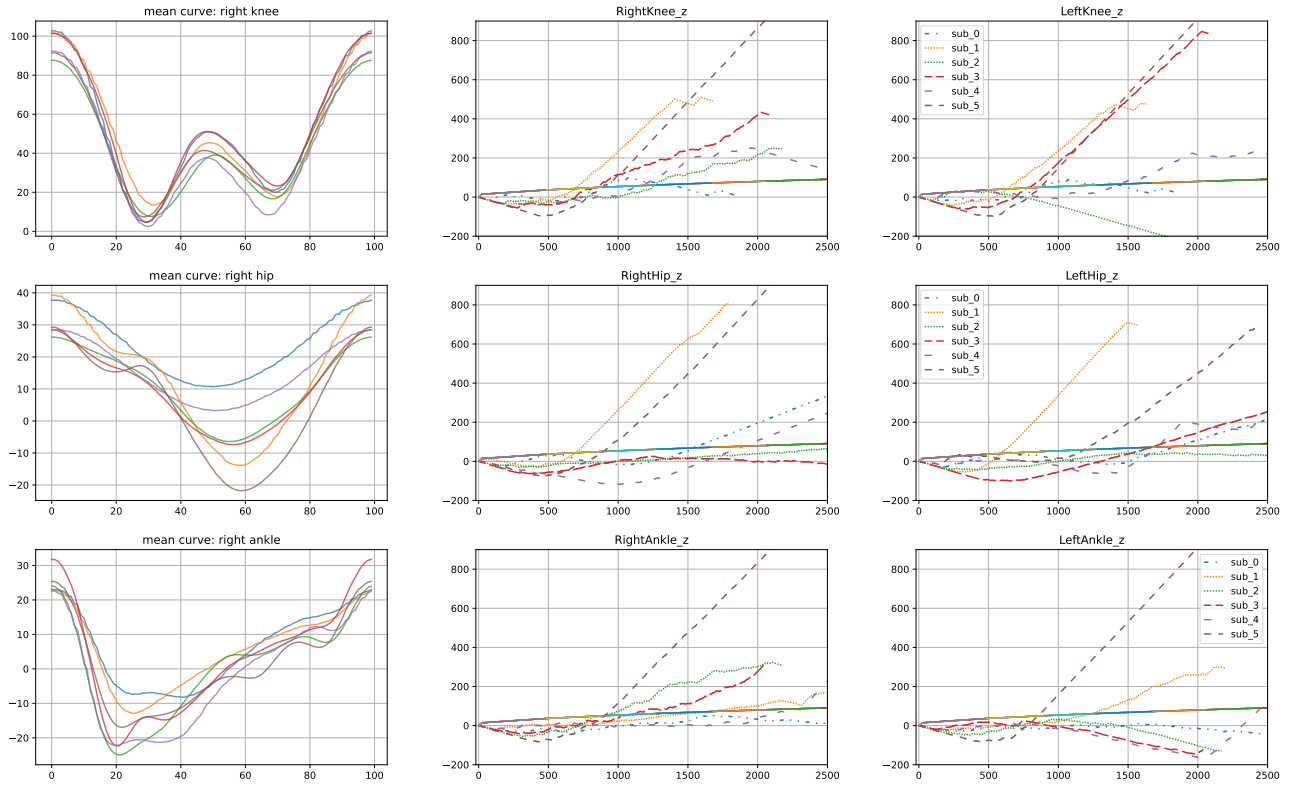


Figure 9: Outdoor fatigue profile of lower extremity joints of all runners. The first column provides the mean curves, second column provides the computations from the right side of the body and the third column provides the computations from the left side of the body.

	subject 0	subject 1	subject 2	subject 3	subject 4	subject 5
Right Knee	48.89	42.36	58.83	41.14	44.76	38.50
Left Knee	49.14	38.93	9.18	38.54	6.25	37.18
Right Hip	10.39	38.98	nan	nan	37.13	38.13
Left Hip	12.01	37.80	nan	40.77	67.85,	8.54
Right Ankle	nan	70.26	42.82	55.06	81.29	38.72
Left Ankle	nan	48.09	nan	nan	93.08	36.49

Table 11: Data from lower extremity joint angles in outdoor setting. Percentage of the run where an up-crossing of the martingale is seen for all the runners.

Contact time of the foot

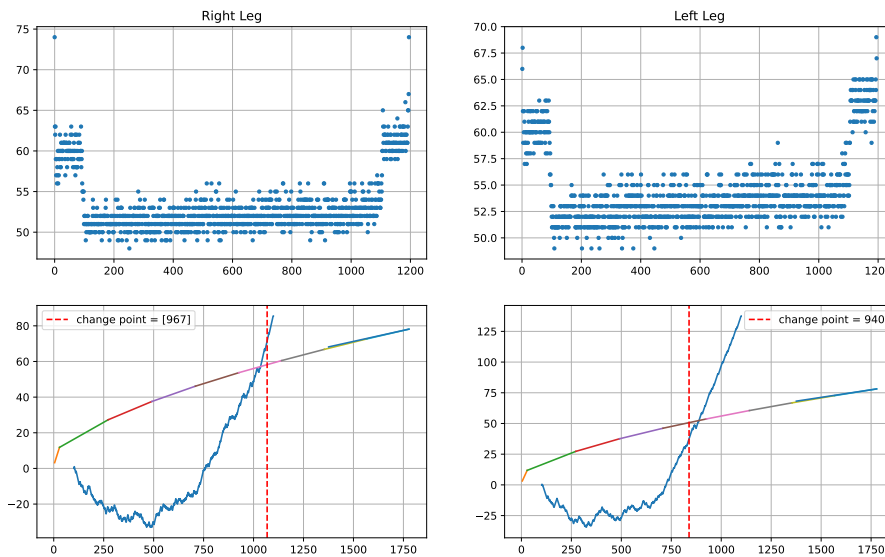


Figure 10: Contact time of the left and right foot of a runner. The runner considered here is the same as Fig. 2. Note that at the initial and final part of the run, the speed is lower and hence the contact time of the foot is longer than in the intermediate part of the run.

8 Proofs of Theorem 1 and Lemma 1.3

8.1 Proof of Lemma 1

Proof of Lemma 1. We will start with deriving one linear bound that holds uniformly for all $t \in \mathbb{N}$. It follows from Example 2, equation (2.29) in Howard et al. (2020)

$$\mathbb{P}_{\mathcal{H}_\infty} \left(\exists t \in \mathbb{N} : M_t \geq x + \underbrace{\frac{x}{2\alpha(1-\alpha)t_0}}_{\text{Linear bound}} (t - \alpha(1-\alpha)t_0) \right) \leq \exp \left\{ -\frac{2x^2}{\alpha(1-\alpha)t_0} \right\}, \quad (18)$$

	subject 0	subject 1	subject 2	subject 3	subject 4	subject 5
Ankle	10.899	48.870	36.911	44.491	44.308	40.588
Knee	37.903	54.590	45.657	45.139	nan	43.442
Hip	12.318	42.285	38.493	40.893	38.966	nan

Table 12: Pooled data (indoor: left, right) joint angles, where the \tilde{D}_i^{\max} (defined in Section 5.8) are used to construct the martingale trajectories. (See Fig. 6 for the corresponding trajectories.)

	subject 0	subject 1	subject 2	subject 3	subject 4	subject 5
Ankle	14.01	51.05	37.93	44.32	nan	40.33
Knee	40.74	59.02	46.60	45.98	48.27	49.35
Hip	81.12	48.12	38.14	41.49	40.28	nan

Table 13: Pooled data from (indoor) left and right joint angles, where where the \tilde{D}_i^{ave} (defined in Section 5.8) are used to construct the martingale trajectories.

	subject 0	subject 1	subject 2	subject 3	subject 4	subject 5
Hip	89.21	48.12	38.32	41.24	40.44	nan
Knee	48.06	85.08	51.58	47.84	45.74	74.35
Ankle	17.00	52.22	38.73	45.08	nan	40.72

Table 14: Pooled data from (indoor) left and right joint angles, where where the \tilde{D}_i^{min} (defined in Section 5.8) are used to construct the martingale trajectories.

	subject 0	subject 1	subject 2	subject 3	subject 4	subject 5
Hip	12.318	42.285	38.493	40.893	38.966	nan
Knee	37.903	54.590	45.657	5.833	nan	43.442
Ankle	10.899	48.870	36.911	44.491	44.308	40.588

Table 15: Pooled data from (outdoor) left and right joint angles, where where the \tilde{D}_i^{max} (defined in Section 5.8) are used to construct the martingale trajectories.

	subject 0	subject 1	subject 2	subject 3	subject 4	subject 5
Hip	6.94	60.78	50.12	23.28	37.08	5.38
Knee	5.02	8.93	8.57	94.08	6.43	7.99
Ankle	5.29	8.20	8.01	19.03	6.84	74.12

Table 16: Cusum: Pooled data from left and right when where the \tilde{D}_i^{max} (defined in Section 5.8) are used to construct the martingale trajectories.

	subject 0	subject 1	subject 2	subject 3	subject 4	subject 5
Ankle	5.34	8.45	27.83	19.20	6.77	8.30
Knee	5.13	8.61	5.40	53.51	6.72	8.31
Hip	6.87	10.68	44.31	25.52	37.82	6.19

Table 17: Cusum: Pooled data from left and right where $\min\{\epsilon_i^l, \epsilon_i^r\}$.

for any $t_0 \in \mathbb{N}$ and $x \in (0, (1 - \alpha)t_0)$. In Eq. (18), we focus on the linear bound as in the following:

$$\begin{aligned}
M_t &\geq x + \frac{x}{2\alpha(1 - \alpha)t_0}(t - \alpha(1 - \alpha)t_0) \\
&= \frac{x}{2\alpha(1 - \alpha)t_0}t + \frac{x}{2} \\
&= \frac{c}{\alpha(1 - \alpha)t_0}t \stackrel{36}{\geq} c,
\end{aligned}$$

	subject 0	subject 1	subject 2	subject 3	subject 4	subject 5
Ankle	5.34	8.45	27.88	19.03	6.77	8.30
Knee	5.08	8.69	6.63	53.51	6.43	7.99
Hip	6.94	72.65	50.12	23.80	37.82	5.43

Table 18: Cusum: Pooled data from left and right, where $\tilde{\epsilon}_i = \text{mean}\{\epsilon_i^l, \epsilon_i^r\}$

when for simplification of notation, $c = x/2$ denotes the intercept of the line and the slope is given by $c/(\alpha(1-\alpha)t_0)$. Further, notice that it follows as a consequence of Example 2.29 of Howard et al. (2020) that $c \in (0, \frac{(1-\alpha)t_0}{2})$. With the appropriate substitutions, Eq. (18) becomes,

$$\mathbb{P}_{\mathcal{H}_\infty} \left(t \in \mathbb{N}, M_t < \frac{c}{\alpha(1-\alpha)t_0}t + c \right) \geq 1 - \exp \left\{ -\frac{8c^2}{\alpha(1-\alpha)t_0} \right\}. \quad (19)$$

We now set $\Delta = \exp \left\{ -\frac{8c^2}{\alpha(1-\alpha)t_0} \right\}$ and solve for c . This gives

$$c = \sqrt{\frac{\alpha(1-\alpha)t_0}{8} \log \left(\frac{1}{\Delta} \right)},$$

and therefore

$$\mathbb{P}_{\mathcal{H}_\infty} \left(t \in \mathbb{N}, M_t < \sqrt{\frac{\log(\frac{1}{\Delta})}{8\alpha(1-\alpha)t_0}}t + \sqrt{\frac{\alpha(1-\alpha)t_0 \log(\frac{1}{\Delta})}{8}} \right) \geq 1 - \Delta,$$

whenever

$$c = \sqrt{\frac{\alpha(1-\alpha)t_0}{8} \log \left(\frac{1}{\Delta} \right)} < \frac{1-\alpha}{2}t_0. \quad (20)$$

Condition (20) is equivalent to the following condition on the parameter t_0

$$t_0 > \frac{\alpha}{2(1-\alpha)} \log \left(\frac{1}{\Delta} \right). \quad (21)$$

The piece-wise linear function is now constructed from the linear bound

$$L_{t_0}(t) = \sqrt{\frac{\log(\frac{1}{\Delta})}{8\alpha(1-\alpha)t_0}}t + \sqrt{\frac{\alpha(1-\alpha)t_0 \log(\frac{1}{\Delta})}{8}},$$

where the linear parts are chosen (i.e., the parameter t_0 is adjusted) such that L_{t_0} is minimal at each of the time points $t = t_1, \dots, t = t_p$. To achieve this optimality property, we now fix $t = t_j, j \geq 1$ and and minimise $L_{t_0}(t_j)$ with respect to t_0 . Elementary calculus

yields one local minimum at $t_{0,\min,j} := t_j/(\alpha(1-\alpha))$, where $L_{t_{0,\min,j}}(t_j) = \sqrt{\frac{1}{2}t_j \log(\frac{1}{\Delta_j})}$. We now establish that $t_{0,\min,j}$ is a global minimum as well for each fixed value of j . Equation (21) provides the lower bound on t_0 of $\frac{\alpha}{2(1-\alpha)} \log(\frac{1}{\Delta})$. We find

$$\lim_{t_0 \rightarrow \frac{\alpha}{2(1-\alpha)} \log(\frac{1}{\Delta_j})} L_{t_0}(t_j) = \frac{1}{2\alpha}t_j + \frac{\alpha}{4} \log(\frac{1}{\Delta_j}),$$

and

$$\sqrt{\frac{1}{2}t_j \log\left(\frac{1}{\Delta_j}\right)} \leq \frac{1}{2\alpha}t_j + \frac{\alpha}{4} \log\left(\frac{1}{\Delta_j}\right) \iff 0 \leq \left(t_j - \frac{\alpha^2}{2} \log\left(\frac{1}{\Delta_j}\right)\right)^2.$$

In addition

$$\lim_{t_0 \rightarrow \infty} L_{t_0}(t_j) = \infty,$$

establishing that the global minima are indeed reached at $t_{0,\min,j}$. Finally, condition (21) needs to be met for all $t_{0,\min,j}$. This is the case if

$$t_{0,\min,j} = \frac{t_j}{\alpha(1-\alpha)} > \frac{\alpha}{2(1-\alpha)} \log\left(\frac{1}{\Delta_j}\right) \iff t_{0,\min,j} \geq \frac{\alpha^2}{2} \log\left(\frac{1}{\Delta_j}\right).$$

We now consider two consecutive linear bounds $L_{t_{0,\min,j}}$ and $L_{t_{0,\min,j+1}}$. Both are valid bounds for all $t \in \mathbb{N}$, however, by construction, $L_{t_{0,\min,j}} \leq L_{t_{0,\min,j+1}}$ for all $t \leq \tau_j$, where τ_j denotes the time point at which both lines intersect (see Figure 11).

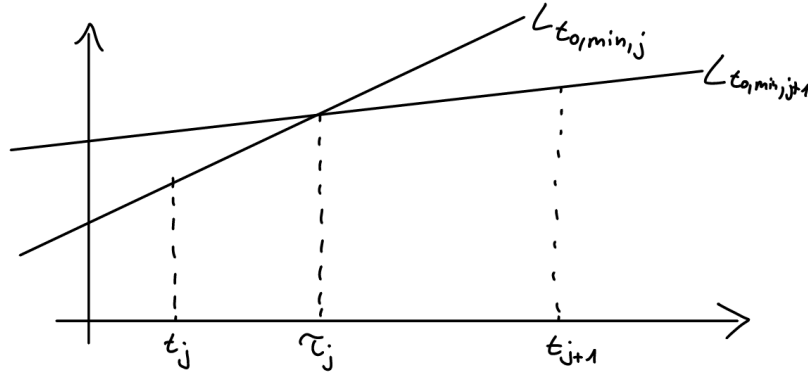


Figure 11: Sketch of the construction of the piece-wise linear bound: Between τ_{j-1} and τ_j the line $L_{t_{0,\min,j}}$ is the smallest of the pre-selected ones. Thereby, choosing $t_{0,j} = t_{0,\min,j}$ and γ^{Linear} as in (11), we obtain the sharpest possible bound by this way of construction. The τ_j 's are obtained by solving the equation $L_{t_{0,\min,j}}(t) = L_{t_{0,\min,j+1}}(t)$ for t .

The piece-wise linear bound is now constructed successively: From the intersection points τ_{j-1} to τ_j , the smallest linear function in this construction is $L_{t_{0,\min,j}}$, which is therefore used as a bound in this range.

We have now established that for each j , the following holds

$$\mathbb{P}(t \in \mathbb{N}, \quad M_t \leq L_{t_{0,\min,j}}(t)) \geq 1 - \Delta_j,$$

which is equivalent to

$$\mathbb{P}(t \in \mathbb{N}, \quad M_t > L_{t_{0,\min,j}}(t) \quad \text{for one } j) \leq \sum_{j=1}^p \Delta_j \leq \delta$$

which implies that the piece-wise linear function $t \mapsto \Gamma_t^{\text{Linear}}$ is a time-uniform bound in the sense of (12).

Remark 4. Obviously, the linear bounds can be fine-tuned in a multitude of ways by adjusting the parameters t_j and Δ_j . For instance, splitting δ into Δ_j 's in such a way that Δ_j is small for small values of j and large for large values of j makes a later detection easier and vice versa. Moreover, choosing a non-equidistant grid of grid points t_j can place more emphasis/accuracy on any domain of choice.

□

8.2 Proof of Theorem 1

Before delving into the lengthy proof of Theorem 1, we provide an outline of the proof strategy in the following steps, also intended to provide a map to the general proof strategy, which is similar to the proof strategy provided for the proof of Theorem 5 in Balsubramani (2014).

8.2.1 Outline of the proof of Theorem 1

The proof of Theorem 1 is split into five lemmas (Lemma 2 - Lemma 6) as outlined below.

1. **Choice of super-martingale (Lemma 2):** We first choose an appropriate super-martingale X_t^λ with additional parameter λ . Such a construction was proposed in (Shafer and Vovk, 2005) in Chapter 5 where they take a game-theoretic approach and M_t is the returns of a player. The strategy was to make the players capital unbounded by defying the law of asymptotic logarithm by choosing appropriate values of λ .
2. **Intuition on additional parameter λ :** As mentioned in (Shafer and Vovk, 2005), for the previous step to work, a number of values of λ have to be considered

such that the indices t where the martingale M_t shows large values (especially those close to $\mathcal{O}(\sqrt{2t \log \log t})$) can be taken advantage of. However, λ is unknown and this is solved by choosing a mixing distribution from which λ may be sampled. In our case, we use a version of a distribution similar to the one proposed in Example 4 of (Robbins and Siegmund, 1970).

3. **Lemma 3:** A moment bound for $|M_t|$ corresponding to a fixed λ_0 is provided.
4. **Lemma 4:** Time-uniform LIL is proved for $\frac{|M_t|}{\sqrt{V_t \log \log V_t}}$ by first controlling the weaker condition $\frac{|M_t|}{\kappa V_t}$, where $V_t = \alpha(1 - \alpha)t$.
5. **Lemma 5:** Then, we prove the moment bound for the case when λ is chosen stochastically. The choice of density function is crucial here.
6. **Lemma 6:** Finally, a stopping time is defined and the Bernstein bound is established.

8.2.2 Statement of Lemma 2 - Lemma 6

Lemma 2. Let the global null hypothesis \mathcal{H}_∞ hold and $\alpha \in (0, 1/2]$. If the $\{\mathbb{1}\{\Phi_i = 1\}\}_{i \in \mathbb{N}}$ are independent and $\{M_t\}_{t \in \mathbb{N}}$ is the martingale defined in (6), the process

$$X_t^\lambda := \exp\{\lambda M_t - \lambda^2 \kappa \alpha(1 - \alpha)t\},$$

is a super-martingale for any $\lambda \in [-e^{-2}, e^{-2}]$, $\alpha \in (0, 1/2]$ and any $\kappa \in [\kappa_0, \infty)$, where

$$\kappa_0 = \frac{\frac{1}{2} + \frac{1}{20e^8} - 0.4\alpha + \max\{\frac{1}{6e^4} - 0.1\alpha, 0\}}{1 - \alpha}.$$

Proof. We need to show that $\mathbb{E}[X_t^\lambda | \mathbb{F}_{t-1}] \leq X_{t-1}^\lambda$ for any $t \in \mathbb{N}$. Since the random variables $\mathbb{1}\{\Phi_t = 1\}$ are independent of \mathbb{F}_{t-1} for any t by assumption, we find

$$\mathbb{E}[\exp(\lambda \xi_t) | \mathbb{F}_{t-1}] = \mathbb{E}[\exp(\lambda(\mathbb{1}\{\Phi_t = 1\} - \alpha)) | \mathbb{F}_{t-1}] = \mathbb{E}[\exp(\lambda(\mathbb{1}\{\Phi_t = 1\} - \alpha))].$$

since $\mathbb{1}\{\Phi_t = 1\}$ is a Bernoulli random variable with success probability α , we obtain

$$\mathbb{E}[\exp(\lambda(\mathbb{1}\{\Phi_t = 1\} - \alpha))] = (1 - \alpha + \alpha e^\lambda) e^{-\lambda \alpha}.$$

This yields

$$\mathbb{E}[X_t^\lambda | \mathbb{F}_{t-1}] = X_{t-1}^\lambda \cdot \exp(-\lambda^2 \kappa \alpha(1 - \alpha) - \alpha \lambda) \cdot (1 - \alpha + \alpha e^\lambda).$$

Set $F(\alpha, \kappa, \lambda) := \exp(-\lambda^2 \kappa \alpha(1 - \alpha) - \alpha \lambda) \cdot (1 - \alpha + \alpha e^\lambda)$. We now show that $\log(F(\alpha, \kappa, \lambda)) \leq 0$ for the parameters within the range specified in the formulation of this lemma.

$$\log(F(\alpha, \kappa, \lambda)) = -\lambda^2 \kappa \alpha(1 - \alpha) - \alpha \lambda + \log(1 - \alpha + \alpha e^\lambda)$$

We now estimate the last term using a Taylor expansion:

$$\log(1 - \alpha + \alpha e^\lambda) \leq \log(1) - \alpha(1 - e^\lambda) - \frac{\alpha^2}{2}(1 - e^\lambda)^2 + \frac{2}{6}\alpha^3(1 - e^\lambda)^3,$$

since $|\alpha(1 - e^\lambda)| < 1$ for all $\alpha \in (0, 1)$. Using the Lagrangian form of the remainder in the Taylor expansion, the first non-zero term can be estimated as follows.

$$-\alpha(1 - e^\lambda) \leq \alpha\lambda + \frac{\alpha\lambda^2}{2} + \frac{\alpha\lambda^3}{6} + \alpha\frac{\lambda^4}{24}e^{\lambda_{\max}}$$

where $\lambda_{\max} = e^{-2}$. This yields

$$-\alpha(1 - e^\lambda) \leq \alpha\lambda + \frac{\alpha\lambda^2}{2} + \frac{\alpha\lambda^3}{6} + \alpha\frac{\lambda^4}{20}e^{\lambda_{\max}},$$

and thus

$$\log(F(\alpha, \kappa, \lambda)) \leq -\lambda^2\kappa\alpha(1 - \alpha) + \frac{\alpha\lambda^2}{2} + \frac{\alpha\lambda^3}{6} + \frac{\alpha\lambda^4}{20} - \frac{\alpha^2}{2}(1 - e^\lambda)^2 + \frac{2}{6}\alpha^3(1 - e^\lambda)^3.$$

If $\lambda > 0$, the last two terms are negative and we can estimate

$$\log(F(\alpha, \kappa, \lambda)) \leq \lambda^2\alpha \left(-\kappa(1 - \alpha) + \frac{1}{2} + \frac{1}{6e^4} + \frac{1}{20e^8} - \frac{\alpha}{2} \right),$$

which gives that $\log(F(\alpha, \kappa, \lambda)) \leq 0$ if

$$\kappa \geq \frac{\frac{1}{2} + \frac{1}{6e^4} + \frac{1}{20e^8} - \frac{\alpha}{2}}{1 - \alpha}.$$

If $\lambda \leq 0$, we find

$$(1 - e^\lambda)^2 = 1 - 2e^\lambda + e^{2\lambda} \geq \lambda^2 + \lambda^3$$

as well as

$$(1 - e^\lambda)^3 \leq -\lambda^3,$$

which implies

$$\begin{aligned} \log(F(\alpha, \kappa, \lambda)) &\leq -\lambda^2\kappa\alpha(1 - \alpha) + \frac{\alpha\lambda^2}{2} + \frac{\alpha\lambda^3}{6} + \frac{\alpha\lambda^4}{23} - \frac{\alpha^2}{2}(\lambda^2 + \lambda^3) - \frac{\lambda^3\alpha^3}{3} \\ &\leq \lambda^2\alpha \left(-\kappa(1 - \alpha) + \frac{1}{2} + \frac{\lambda^2}{23} - \frac{\alpha}{2} + \frac{2}{3}\alpha|\lambda| \right) \\ &\leq \lambda^2\alpha \left(-\kappa(1 - \alpha) + \frac{1}{2} + \frac{1}{20e^8} - 0.4\alpha \right). \end{aligned}$$

From this we conclude that for $\lambda < 0$ $\log(F(\alpha, \kappa, \lambda)) \leq 0$ if

$$\kappa \geq \frac{\frac{1}{2} + \frac{1}{20e^8} - 0.4\alpha}{1 - \alpha}.$$

The statement of the lemma now follows. □

Lemma 3. For any stopping time τ , $\kappa \geq \kappa_0$, and a fixed $\lambda_0 \in [-e^{-2}, e^{-2}]$, we have that,

$$\mathbb{E}[\exp(\lambda_0 M_\tau - \lambda_0^2 \kappa V_\tau)] \leq 1.$$

Proof. The statement of the lemma follows directly by the optional stopping theorem. \square

Lemma 4. Let $k \in (0, 1)$, $\kappa \geq \kappa_0$, and $t_0 = \left\lceil \frac{1}{\lambda_0^2 \kappa \alpha (1-\alpha)} \log\left(\frac{1}{\delta}\right) \right\rceil$ with $|\lambda_0| \leq e^{-2}/(1+\sqrt{k})$. Fix any $\delta > 0$. Then, the following holds

$$\mathbb{P}\left(\frac{M_t}{\kappa \alpha (1-\alpha)t} \leq 2\lambda_0 \quad \text{for all } t \geq t_0\right) \geq 1 - \delta.$$

Equivalently put, with the definition of the set

$$A_\delta = \left\{ \omega \in \Omega : \frac{M_t}{\kappa \alpha (1-\alpha)t} \leq 2\lambda_0, \forall t \geq t_0 \right\},$$

the statement of the above becomes

$$\mathbb{P}(A_\delta) \geq 1 - \delta.$$

Proof. Define the stopping time $\tau_1 = \min\{t \geq t_0 : \frac{M_t}{\kappa \alpha (1-\alpha)t} > 2\lambda_0\}$. Then it suffices to prove that $\mathbb{P}(\tau_1 < \infty) \leq \delta$ i.e., uniformly for all $t \geq t_0$, the rescaled martingale $\frac{M_t}{\kappa \alpha (1-\alpha)t} \leq 2\lambda_0$ with high probability. For this purpose, we use the previous lemma and get that,

$$\begin{aligned} 1 &\geq \mathbb{E}[\exp(\lambda_0 M_t - \lambda_0^2 \kappa \alpha (1-\alpha)t)] \\ &\geq \mathbb{E}[\exp(\lambda_0 M_t - \lambda_0^2 \kappa \alpha (1-\alpha)t) | \tau_1 < \infty] \mathbb{P}(\tau_1 < \infty) \\ &> \mathbb{E}[\exp\{\lambda_0^2 \kappa \alpha (1-\alpha) \tau_1\} | \tau_1 < \infty] \mathbb{P}(\tau_1 < \infty). \end{aligned}$$

where the last estimate holds because $M_{\tau_1} > 2\lambda_0 \kappa \alpha (1-\alpha) \tau_1$ for $\tau_1 < \infty$. Since $\tau_1 \geq t_0$ by construction, we further obtain

$$\begin{aligned} 1 &\geq \mathbb{E}[\exp\{\lambda_0^2 \kappa \alpha (1-\alpha) t_0\} | \tau_1 < \infty] \mathbb{P}(\tau_1 < \infty) \\ &> \mathbb{E}[\exp\{-\log(\delta)\} | \tau_1 < \infty] \mathbb{P}(\tau_1 < \infty) \geq \frac{1}{\delta} \mathbb{P}(\tau_1 < \infty), \end{aligned}$$

Therefore, $\mathbb{P}(\tau_1 < \infty) \leq \delta$, which concludes the proof of this lemma. \square

We continue with Step 4 from our outline i.e., we prove the moment bound for the case when λ is chosen stochastically. In the following, $\mathbb{E}[\cdot]$ denotes expectation with respect to the original probability space, $\mathbb{E}^\lambda[\cdot]$ denotes expectation with respect to the probability

space $(\Omega_\lambda, \mathbb{F}_\lambda, \mathbb{P}_\lambda)$ and, for any event $A \in \mathbb{F}$, $\mathbb{E}_A[\cdot]$ denotes conditional expectation $\mathbb{E}[\cdot|A]$, i.e.,

$$\mathbb{E}_A[X] = \frac{1}{\mathbb{P}(A)} \int_A X \, d\mathbb{P}.$$

With the latter notation, we can now state our next lemma.

Lemma 5. Given that $X_t^\lambda := \exp\{\lambda M_t - \lambda^2 \kappa \alpha (1 - \alpha)t\}$ is a super-martingale for any $\lambda \in [-e^{-2}, e^{-2}]$ if $\kappa \geq \kappa_0$) and that λ is sampled, independently of $\mathbf{1}\{\Phi_1 = 1\}, \mathbf{1}\{\Phi_2 = 1\}, \dots$ from $(\Omega_\lambda, \mathbb{F}_\lambda, \mathbb{P}_\lambda)$, with density $f(\lambda) = 1/(|\lambda|(-\log|\lambda|)^2)$ on $\lambda \in [-e^{-2}, e^{-2}] \setminus \{0\}$, it holds that

$$\mathbb{E}_{B_\delta}[\mathbb{E}^\lambda[X_t^\lambda]] \geq \mathbb{E}_{B_\delta} \left[\frac{\exp \left\{ \frac{M_t^2}{4\kappa V_t} (1 - k) \right\}}{\log^2 \left(\frac{2\kappa V_t}{|M_t|(1 - \sqrt{k})} \right)} \right],$$

where

$$B_\delta := \left\{ \omega \in \Omega : \frac{|M_t|}{\kappa \alpha (1 - \alpha)t} \leq 2\lambda_0, \forall t \geq t_0 \right\}, \quad \lambda_0 \in \left(0, e^{-2} / (1 + \sqrt{k}) \right).$$

Proof. Let λ be chosen stochastically from $(\Omega_\lambda, \mathbb{F}_\lambda, \mathbb{P}_\lambda)$ with probability density f such that $f(\lambda) = \frac{1}{|\lambda|(\log \frac{1}{|\lambda|})^2}$ on $\lambda \in [-e^{-2}, e^{-2}] \setminus \{0\}$, a mixing distribution suggested in Robbins and Siegmund (1970). Then, with $V_t = \alpha(1 - \alpha)t$

$$\begin{aligned} \mathbb{E}^\lambda[X_t^\lambda] &= \int_{-1/e^2}^{1/e^2} \exp(\lambda M_t - \lambda^2 \kappa V_t) f(\lambda) d\lambda \\ &= \int_{-1/e^2}^{1/e^2} \exp \left\{ \frac{M_t^2}{4\kappa V_t} - \lambda^2 \kappa V_t - \frac{M_t^2}{4\kappa V_t} + \lambda M_t \right\} f(\lambda) d\lambda \\ &= \exp \left\{ \frac{M_t^2}{4\kappa V_t} \right\} \int_{-1/e^2}^{1/e^2} \exp \left\{ -\kappa V_t \left(\lambda^2 + \frac{M_t^2}{4\kappa^2 V_t^2} - \frac{\lambda M_t}{\kappa V_t} \right) \right\} f(\lambda) d\lambda. \end{aligned}$$

This yields

$$\begin{aligned} \mathbb{E}^\lambda[X_t^\lambda] &= \exp \left\{ \frac{M_t^2}{4\kappa V_t} \right\} \int_{-1/e^2}^{1/e^2} \exp \left\{ -\kappa V_t \left(\lambda - \frac{M_t}{2\kappa V_t} \right)^2 \right\} f(\lambda) d\lambda \\ &= \exp \left\{ \frac{M_t^2}{4\kappa V_t} \right\} \int_{-1/e^2}^0 \exp \left\{ -\kappa V_t \left(\lambda - \frac{M_t}{2\kappa V_t} \right)^2 \right\} f(\lambda) d\lambda \\ &\quad + \exp \left\{ \frac{M_t^2}{4\kappa V_t} \right\} \int_0^{1/e^2} \exp \left\{ -\kappa V_t \left(\lambda - \frac{M_t}{2\kappa V_t} \right)^2 \right\} f(\lambda) d\lambda. \end{aligned}$$

By a change of variables, using that $f(\lambda) = f(-\lambda)$, we find

$$\begin{aligned}\mathbb{E}^\lambda[X_t^\lambda] &= \exp\left\{\frac{M_t^2}{4\kappa V_t}\right\} \int_0^{1/e^2} \exp\left\{-\kappa V_t\left(-\lambda - \frac{M_t}{2\kappa V_t}\right)^2\right\} f(\lambda) d\lambda \\ &\quad + \exp\left\{\frac{M_t^2}{4\kappa V_t}\right\} \int_0^{1/e^2} \exp\left\{-\kappa V_t\left(\lambda - \frac{M_t}{2\kappa V_t}\right)^2\right\} f(\lambda) d\lambda.\end{aligned}$$

Since both integrals are non-negative, we obtain

$$\mathbb{E}^\lambda[X_t^\lambda] \geq \exp\left\{\frac{M_t^2}{4\kappa V_t}\right\} \int_0^{1/e^2} \exp\left\{-\kappa V_t\left(\lambda - \frac{|M_t|}{2\kappa V_t}\right)^2\right\} f(\lambda) d\lambda.$$

Notice that the exponential in the integral is maximal, i.e.,

$$\exp\left\{-\kappa V_t\left(\lambda - \frac{|M_t|}{2\kappa V_t}\right)^2\right\} = 1,$$

if $\lambda = |M_t|/(2\kappa V_t)$. To further estimate the integral, we therefore restrict the integral over a region around $\lambda = |M_t|/(2\kappa V_t)$ and find for $k \in (0, 1)$

$$\mathbb{E}^\lambda[X_t^\lambda] \geq \exp\left\{\frac{M_t^2}{4\kappa V_t}\right\} \int_{\frac{|M_t|}{2\kappa V_t}(1-\sqrt{k})}^{\frac{|M_t|}{2\kappa V_t}(1+\sqrt{k})} \exp\left\{-\kappa V_t\left(\lambda - \frac{|M_t|}{2\kappa V_t}\right)^2\right\} f(\lambda) d\lambda.$$

Notice that on the set B_δ , we have for $k \in (0, 1)$ that

$$\left(\frac{|M_t|}{2\kappa V_t}(1-\sqrt{k}), \frac{|M_t|}{2\kappa V_t}(1+\sqrt{k})\right) \subset (0, e^{-2}),$$

i.e., the domain of integration is included in the support of \mathbb{P}_λ if we remain on the set B_δ , which we assume in the following. Now, the exponential in the integral is lower bounded by $\exp\left\{-k\frac{M_t^2}{4\kappa V_t}\right\}$, which yields

$$\begin{aligned}\mathbb{E}^\lambda[X_t^\lambda] &\geq \exp\left\{\frac{M_t^2}{4\kappa V_t} - k\frac{M_t^2}{4\kappa V_t}\right\} \int_{\frac{|M_t|}{2\kappa V_t}(1-\sqrt{k})}^{\frac{|M_t|}{2\kappa V_t}(1+\sqrt{k})} f(\lambda) d\lambda \\ &= \exp\left\{(1-k)\frac{M_t^2}{4\kappa V_t}\right\} \left[\frac{1}{\log(\frac{1}{\lambda})}\right]_{\frac{|M_t|}{2\kappa V_t}(1-\sqrt{k})}^{\frac{|M_t|}{2\kappa V_t}(1+\sqrt{k})}.\end{aligned}$$

Finally,

$$\mathbb{E}^\lambda[X_t^\lambda] \geq \exp\left\{\frac{M_t^2}{4\kappa V_t}(1-k)\right\} \frac{\log\left(\frac{1+\sqrt{k}}{1-\sqrt{k}}\right)}{\log^2\left(\frac{2\kappa V_t}{|M_t|(1-\sqrt{k})}\right)}.$$

Taking τ to be any stopping time and using the definition of B_δ for $t \geq \tau$, we get that,

$$\begin{aligned}\mathbb{E}_{B_\delta}[\mathbb{E}^\lambda[X_\tau^\lambda]] &\geq \mathbb{E}_{B_\delta} \left[\exp \left\{ \frac{M_t^2}{4\kappa V_t} (1-k) \right\} \frac{\log \left(\frac{1+\sqrt{k}}{1-\sqrt{k}} \right)}{\log^2 \frac{2\kappa V_t}{|M_t|(1-\sqrt{k})}} \right] \\ &= \mathbb{E}_{B_\delta} \left[\frac{\mathcal{K} \exp \left\{ \frac{M_t^2}{4\kappa V_t} (1-k) \right\}}{\log^2 \left(\frac{2\kappa V_t}{|M_t|(1-\sqrt{k})} \right)} \right].\end{aligned}$$

where $\mathcal{K} := \log \left(\frac{1+\sqrt{k}}{1-\sqrt{k}} \right)$. □

Lemma 6. Let $k \in (0, 1)$, $\kappa \geq \kappa_0$, $\mathcal{K} = \log \left(\frac{1+\sqrt{k}}{1-\sqrt{k}} \right)$, $\lambda_0 \in (0, e^{-2}/(1+\sqrt{k}))$ and $V_t = \alpha(1-\alpha)t$. Define a stopping time τ as

$$\begin{aligned}\tau = \min \left\{ t \geq t_0 : M_t > 2\lambda_0\kappa V_t \vee \right. \\ \left. \left(M_t \leq 2\lambda_0\kappa V_t \wedge M_t > \sqrt{\frac{1}{1-k}\kappa V_t \left(2 \log \log \frac{\kappa V_t}{|M_t|(1-\sqrt{k})} + \log \frac{2}{\delta\mathcal{K}} \right)} \right) \right\}.\end{aligned}$$

Then, it holds that,

$$P(\tau = \infty) \geq 1 - \delta.$$

Proof. At stopping time τ , we can bound the martingale M_t from below by

$$M_t > \sqrt{\frac{4}{1-k}\kappa V_t \left(2 \log \log \frac{2\kappa V_t}{|M_t|(1-\sqrt{k})} + \log \frac{2}{\delta\mathcal{K}} \right)}.$$

This implies

$$\begin{aligned}\frac{M_t^2(1-k)}{4\kappa V_t} &> 2 \log \log \left(\frac{2\kappa V_t}{|M_t|(1-\sqrt{k})} \right) + \log \frac{2}{\delta\mathcal{K}} \\ \Leftrightarrow \exp \left\{ \frac{M_t^2(1-k)}{4\kappa V_t} \right\} &> \frac{2}{\delta\mathcal{K}} \log^2 \left(\frac{2\kappa V_t}{|M_t|(1-\sqrt{k})} \right),\end{aligned}$$

and finally

$$\frac{\mathcal{K} \exp \left\{ \frac{M_t^2(1-k)}{4\kappa V_t} \right\}}{\log^2 \left(\frac{2\kappa V_t}{|M_t|(1-\sqrt{k})} \right)} > \frac{2}{\delta}. \quad (22)$$

Using the previous lemma, on the event $B_{\delta/2}$, we have that,

$$\begin{aligned}
\frac{4}{3} &\geq \frac{1}{1 - \frac{\delta}{2}} = \frac{\mathbb{E}^\lambda[\mathbb{E}[X_0^\lambda]]}{1 - \frac{\delta}{2}} \stackrel{(i)}{\geq} \frac{\mathbb{E}^\lambda[\mathbb{E}[X_\tau^\lambda]]}{1 - \frac{\delta}{2}} \geq \mathbb{E}^\lambda[\mathbb{E}_{B_{\delta/2}}[X_\tau^\lambda]] \stackrel{(ii)}{=} \mathbb{E}_{B_{\delta/2}}[\mathbb{E}^\lambda[X_\tau^\lambda]] \\
&\stackrel{(iii)}{\geq} \mathbb{E}_{B_{\delta/2}} \left[\frac{\mathcal{K} \exp \left\{ \frac{|M_\tau|^2(1-k)}{4\kappa V_\tau} \right\}}{\log^2 \left(\frac{2\kappa V_\tau}{|M_\tau|(1-\sqrt{k})} \right)} \right] \geq \mathbb{E}_{B_{\delta/2}} \left[\frac{\mathcal{K} \exp \left\{ \frac{|M_\tau|^2(1-k)}{4\kappa V_\tau} \right\}}{\log^2 \left(\frac{2\kappa V_\tau}{|M_\tau|(1-\sqrt{k})} \right)} \middle| \tau < \infty \right] P_{B_{\delta/2}}(\tau < \infty) \\
&\stackrel{(iv)}{>} \frac{2}{\delta} P_{B_{\delta/2}}(\tau < \infty),
\end{aligned}$$

where (i) is due to the optional stopping theorem, (ii) follows from Tonelli's theorem, (iii) is due to the Lemma 5 for fixed $\lambda \in (e^{-2}, e^{-2})$ and (iv) follows from (22). We deduce that

$$P_{B_{\delta/2}}(\tau < \infty) < \frac{2}{3}\delta.$$

Next, we need to relate $P_{B_{\delta/2}}(\tau < \infty)$ to $P_{A_{\delta/2}}(\tau < \infty)$. Since $B_\delta \subset A_\delta$, clearly

$$\frac{1}{P(A_\delta)} \leq \frac{1}{P(B_\delta)}.$$

Furthermore,

$$\begin{aligned}
P(\{\tau < \infty\} \cap A_\delta) &= P((\{\tau < \infty\} \cap B_\delta) \cup (\{\tau < \infty\} \cap \{M_t < -2\lambda_0\kappa V_t\})) \\
&= P(\{\tau < \infty\} \cap B_\delta) + P(\{\tau < \infty\} \cap \{M_t < -2\lambda_0\kappa V_t\}).
\end{aligned}$$

Since $\{\tau < \infty\} \cap \{M_t < -2\lambda_0\kappa V_t\} = \emptyset$, we conclude

$$P(\{\tau < \infty\} \cap A_\delta) = P(\{\tau < \infty\} \cap B_\delta).$$

Therefore, we have,

$$\frac{2}{3}\delta \geq P_{B_{\delta/2}}(\tau < \infty) \geq P_{A_{\delta/2}}(\tau < \infty).$$

Next,

$$P_{A_{\delta/2}}(\tau < \infty) < \frac{2}{3}\delta \implies P_{A_{\delta/2}}(\tau = \infty) \geq 1 - \frac{2}{3}\delta.$$

Further, since $\delta < \frac{1}{2}$ by assumption, we have that,

$$\begin{aligned}
P(\tau = \infty) &\geq P(\tau = \infty \cap A_{\delta/2}) \stackrel{(i)}{=} P_{A_{\delta/2}}(\tau = \infty)P(A_{\delta/2}) \\
&\stackrel{(ii)}{\geq} \left(1 - \frac{2}{3}\delta\right) \left(1 - \frac{\delta}{2}\right) \geq 1 - \delta,
\end{aligned}$$

where (i) follows from the definition of A_δ and (ii) follows from Lemma 4. \square

8.2.3 Proof of the theorem

The claim of Theorem 1 is an immediate consequence of Lemma 6, where the bound on κ follows from the requirement that X_t^λ is a super-martingale and $s_{0,\text{LIL}}$ results from choosing the largest possible value for λ_0 that is in agreement with Lemma 2 - Lemma 6, i.e., $\lambda_0 = e^{-2}/(1 + \sqrt{k})$ for the initial time t_0 defined in Lemma 4.

□